Supporting Information

Enantio-enriched CPL-active helicene-bipyridine-rhenium complexes

Nidal Saleh,[a] Monika Srebro,[b] Thibault Reynaldo, [a] Nicolas Vanthuyne,[c] Loïc Toupet,[a] Victoria Y. Chang, [d] G. Muller,[d] J. A. Gareth Williams,[e] Christian Roussel,[c] Jochen Autschbach,*[,f] Jeanne Crassous*[,a]

A. Computational part

Computational details

The computational protocol employed in this study followed that established in previous research on transition-metal-based systems with helicene ligands.[1] Namely, DFT geometry optimizations and subsequent TDDFT optical rotation (OR) and circular dichroism (CD) calculations were performed with the Turbomole package, versions 5.7.1 and 6.5,[2] at the BP[3] and BHLYP[4] level respectively, using SV(P) basis set[5] along with a 60-electron scalar relativistic effective core potential for Re atoms.[6] Solvent effects (dichloromethane, DCM, $\varepsilon = 8.9$) were included in the calculations via the conductor-like screening model (COSMO)[7] with the default parameters of the Turbomole/COSMO implementation.

The OR parameters β were computed at the sodium *D*-line wavelength $\lambda = 589.3$ nm. Reported values of molar rotations were obtained from β calculated in atomic units, for the light frequency $\tilde{\nu} = 1/\lambda$ given in cm^{-1}, using the numerical conversion (eq. 1):

$$[\phi] = 1.342219 \cdot 10^{-2} \tilde{\nu}^2 \beta(\tilde{\nu})$$

The CD calculations covered 100 lowest singlet excited states. The simulated spectra were obtained as the sums of Gaussian functions centered at the vertical singlet excitation energies and scaled using the calculated rotatory strengths[8] with a $\sigma = 0.2$ eV parameter used as the root mean square width.

Electronic emission spectra via S_1 and T_1 excited-states geometry optimizations were obtained using the Gaussian 09 program[9] with BHLYP/SV(P), and polarizable continuum model (PCM)[7c,10] to simulate the solvent (DCM) effects. In the case of triplet states calculations, the Tamm-Dancoff approximation (TDA)[11] was applied, as for BHLYP it was shown to provide more reliable results than the full TDDFT.

Radiative lifetime calculations were performed at TDDFT-TDA BHLYP/SV(P)/COSMO(DCM) optimized T_1 structures using TDDFT with perturbative (p) and self-consistent inclusion of spin-orbit coupling, pSOC-TDDFT[12] and SOC-TDDFT,[13] respectively, as implemented in Amsterdam Density Functional (ADF) package, version 2013.01.[14] A full (self-consistent) SOC-TDDFT is theoretically the more accurate approach. The BHLYP and B3LYP[4a,15] functionals along with a Slater-type orbital basis set, relativistic all-electron triple-ξ polarization (TZP) for Re, double-ξ polarization (DZP) for Cl, O, N, C, and double-ξ (DZ) basis set for H, were employed. Solvent (DCM) effects were included via COSMO approach with the default parameters of the ADF/COSMO implementation.[16] A general protocol along with technical settings of those calculations followed that employed in recent benchmark studies on phosphorescent lifetimes and zero-field splitting of organometallic complexes by Mori et al.[17] which identified B3LYP SOC-TDDFT with COSMO approach as a robust method to reproduce experimental emission lifetimes. The averaged radiative lifetime τ_{av} at a given temperature T was calculated based on the individual radiative decay times τ_i from i-th substrate (i = 1, 2, 3) of the T_1 state to the ground state and the relative energies $\Delta E_{i\text{-}1}$ of the T_1 substrates with respect to the lowest-energy substrate, employing a Boltzmann average (eq. 2):

$$\tau_{av} = \frac{1}{k_{av}} = \frac{\sum_i e^{-(\Delta E_{i-1}/k_B T)}}{\sum_i k_i \cdot e^{-(\Delta E_{i-1}/k_B T)}}$$

with the i-th radiative rate $k_i = \dfrac{1}{\tau_i}$.

All the calculations were carried out without imposing symmetry. For the cationic helicene-bipyridine-rhenium(I) complexes **3b**$^{\mathbf{1,2}}$, counterions were neglected in the calculations.

Additional computational results

Table S1. Experimental and calculated molar rotations, $[\phi]_D$, (in degree cm^2/dmol) of enantiopure helicene-bipyridine-rhenium complexes, (*P*,*C*^{Re})-**2b^1** and (*P*,*A*^{Re})-**2b^2**, along with their parent ligand, *P*-**1b**.

Method	**1b**	**2b^1**	**2b^2**
BHLYP/SV(P)/gas-phase	15047	11961	10435
BHLYP/SV(P)/COSMO [a]	14176	12721	11888
Expt. (23°C) [a]	12000	9260	10260

[a] Dichloromethane (DCM, ε = 8.9) solvent.

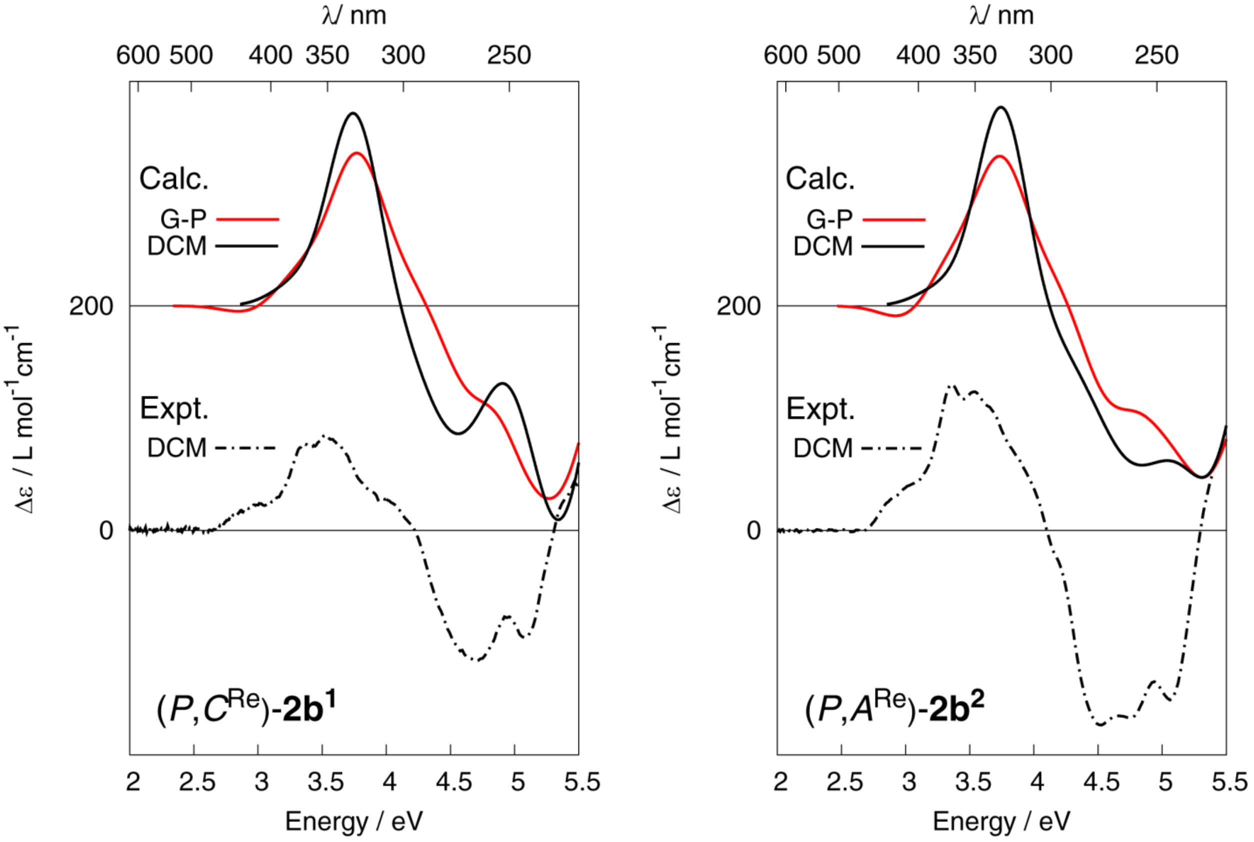

Figure S1. Comparison of the experimental (dashed lines) and TDDFT BHLYP/SV(P) (solid lines) CD spectra of helicene-bipyridine-rhenium complexes, (*P*,*C*^{Re})-**2b^1** and (*P*,*A*^{Re})-**2b^2**. No spectral shift has been applied. G-P: gas-phase, DCM: dichloromethane solvent calculations.

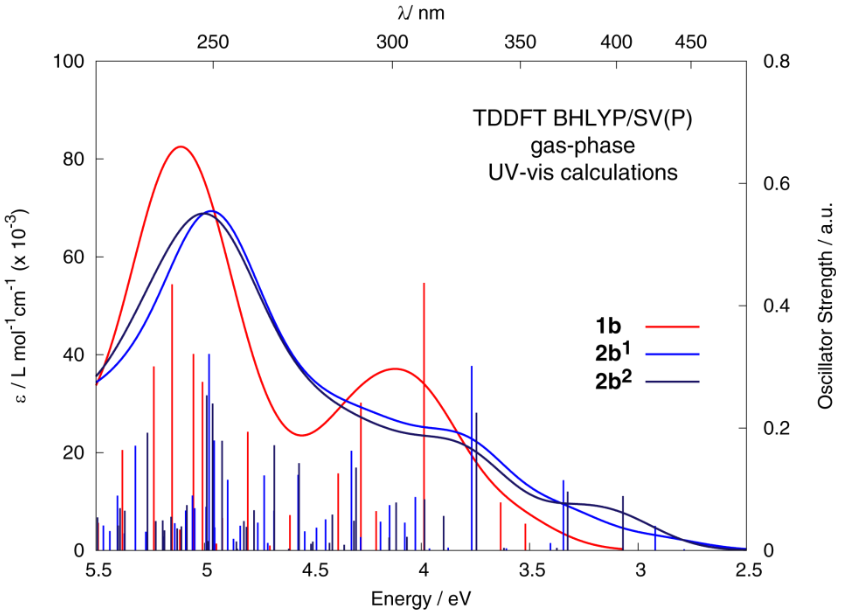

Figure S2. Comparison of the simulated (BHLYP/SV(P)/gas-phase) UV-vis spectra of **1b** (red line), **2b**^{1} (light blue line), and **2b**^{2} (dark blue line). No spectral shift has been applied. Calculated excitation energies and oscillator strengths indicated as 'stick' spectra.

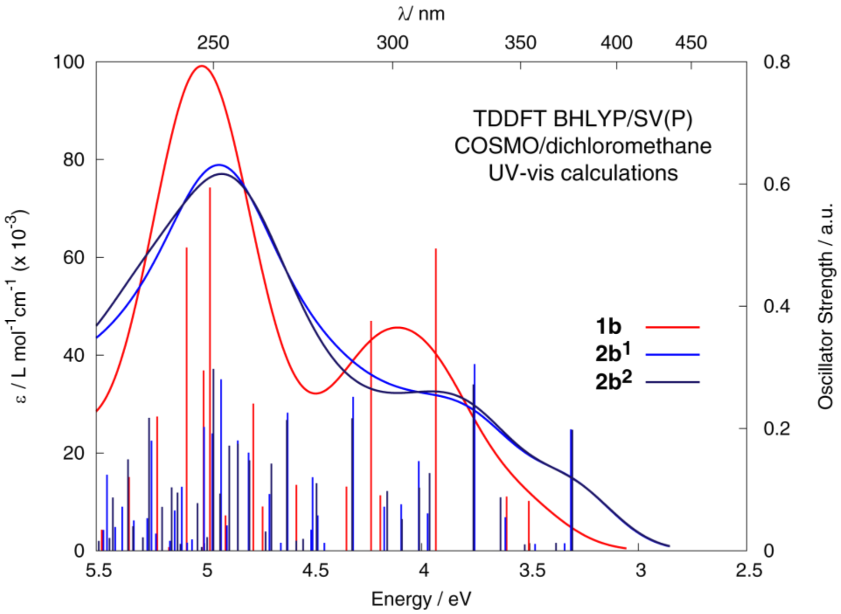

Figure S3. Comparison of the simulated (BHLYP/SV(P)/COSMO(DCM)) UV-vis spectra of **1b** (red line), **2b**^{1} (light blue line), and **2b**^{2} (dark blue line). No spectral shift has been applied. Calculated excitation energies and oscillator strengths indicated as 'stick' spectra.

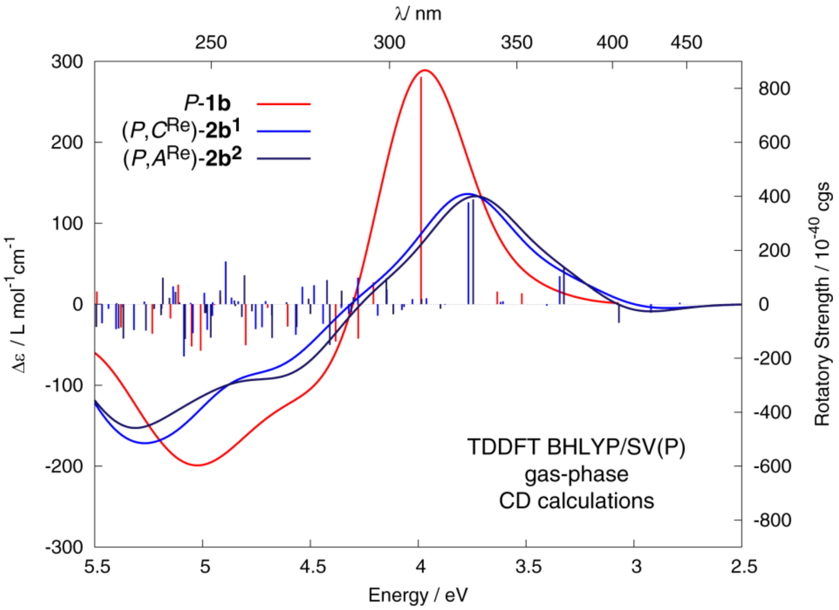

Figure S4. Comparison of the simulated (BHLYP/SV(P)/gas-phase) CD spectra of *P*-**1b** (red line), (*P*,*C*^{Re})-**2b**^{1} (light blue line), and (*P*,*A*^{Re})-**2b**^{2} (dark blue line). No spectral shift has been applied. Calculated excitation energies and rotatory strengths indicated as 'stick' spectra.

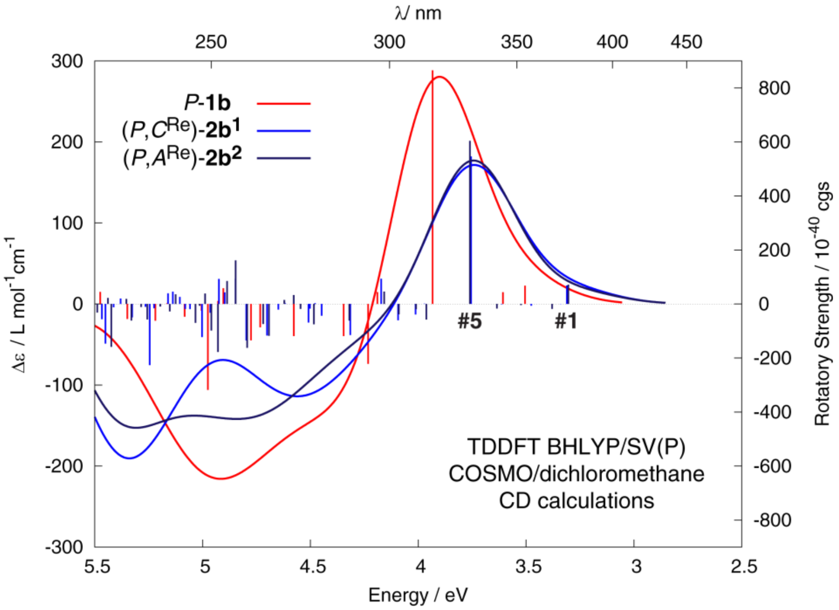

Figure S5. Comparison of the simulated (BHLYP/SV(P)/COSMO(DCM)) CD spectra of *P*-**1b** (red line), (*P*,*C*^{Re})-**2b**^{1} (light blue line), and (*P*,*A*^{Re})-**2b**^{2} (dark blue line). No spectral shift has been applied. Calculated excitation energies and rotatory strengths indicated as 'stick' spectra. Numbered excitations correspond to those analyzed in detail. For assignment of the CD spectrum for *P*-**1b** see ref. 1f.

Table S2. Selected dominant excitations and occupied (occ) – unoccupied (unocc) MO pair contributions (greater than 10%) of (*P*,*C*$^{\mathrm{Re}}$)-**2b**$^{\mathbf{1}}$ and (*P*,*A*$^{\mathrm{Re}}$)-**2b**$^{\mathbf{2}}$. BHLYP/SV(P)/COSMO(DCM) calculations.

Excitation	E / eV	λ / nm	f	R / 10^{-40} cgs	occ no.	unocc no.	%
				2b$^{\mathbf{1}}$			
#1	3.31	374	0.1985	68.87	143	144	51.1
					142	144	18.4
#5	3.76	330	0.3055	546.52	143	145	43.3
					142	145	24.6
				2b$^{\mathbf{2}}$			
#1	3.30	375	0.1978	71.38	143	144	60.0
					142	144	11.2
#5	3.76	330	0.2720	604.03	143	145	41.4
					142	145	24.8

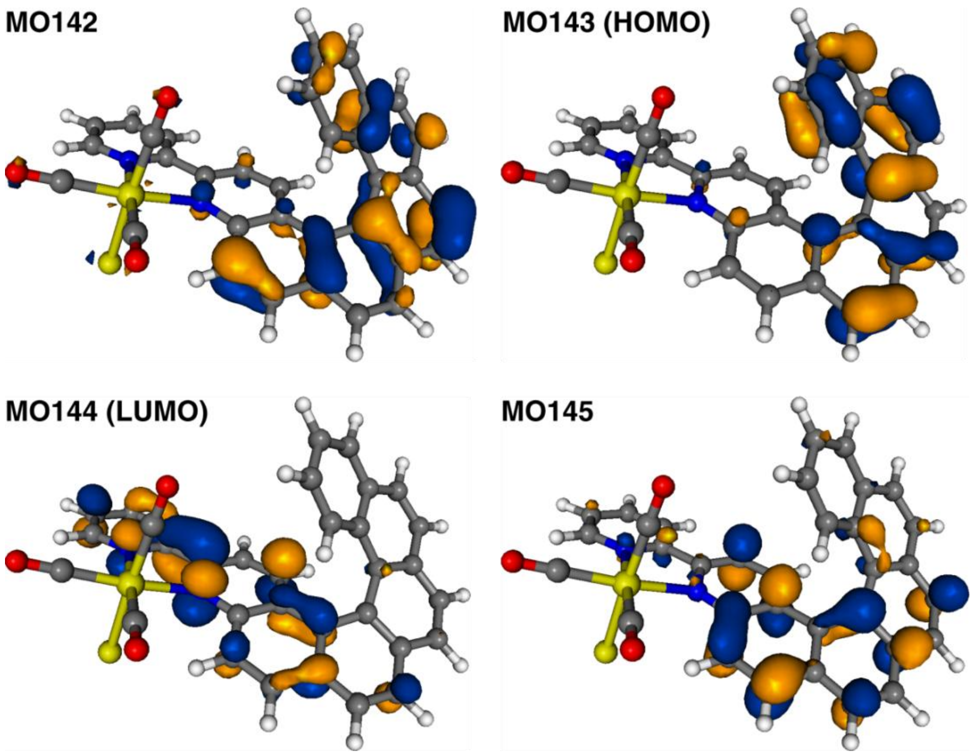

Figure S6. Isosurfaces (0.04 au) of MOs involved in selected transitions of **2b**$^{\mathbf{1}}$. BHLYP/SV(P)/COSMO(DCM) calculations.

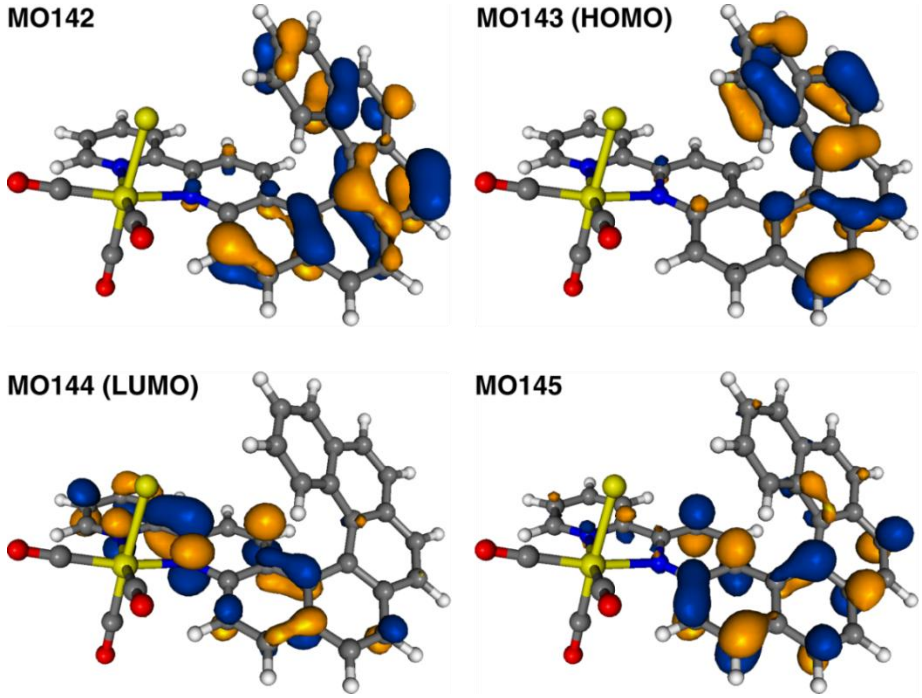

Figure S7. Isosurfaces (0.04 au) of MOs involved in selected transitions of **2b^2**. BHLYP/SV(P)/COSMO(DCM) calculations.

Table S3. Calculated molar rotations, $[\phi]_D$, (in degree cm^2/dmol) of enantiopure helicene-bipyridine-rhenium complexes, (P,C^{Re})-**3b^1** and (P,A^{Re})-**3b^2**, along with experimental data for unresolved mixture of (P,C^{Re})-**3b^1** and (P,A^{Re})-**3b^2**.

Method	System	Conformer [a]	ΔE [b]	$[\phi]_D$
BHLYP/SV(P)/COSMO [c]	**3b^1**	1	0.00	15006
		2	0.06	13110
		3	0.44	13643
		4	0.40	16477
	3b^2	1	0.57	13211
		2	0.60	11546
	3b^{1,2}			14034 [d]
Expt. (23°C) [c]	**3b^{1,2}**			15040

[a] Compare Figure S8. [b] BP/SV(P)/COSMO relative energy ΔE, in kcal/mol, with respect to the lowest-energy conformer of (P,C^{Re})-**3b^1**, **3b^1-1**. [c] Dichloromethane (DCM, ε = 8.9) solvent. [d] Boltzmann averaged value at 23°C based on conformers listed above in the table.

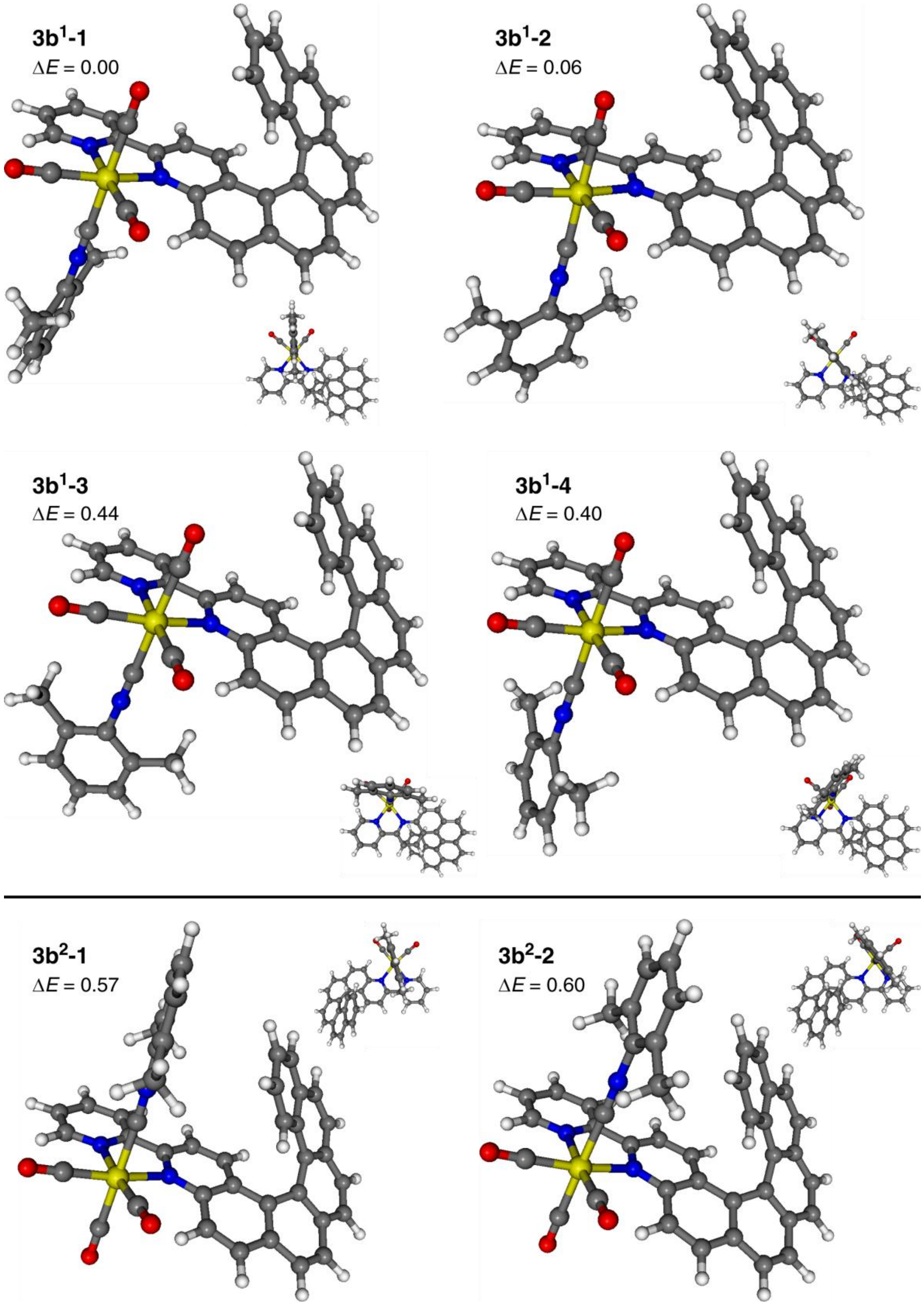

Figure S8. Selected low-energy optimized structures of helicene-bipyridine-rhenium complex, (P,C^{Re})-**3b^1** (top) and (P,A^{Re})-**3b^2** (bottom). Relative energy ΔE (in kcal/mol) with respect to the lowest-energy conformer of (P,C^{Re})-**3b^1**. BP/SV(P)/COSMO(DCM) calculations without counterion.

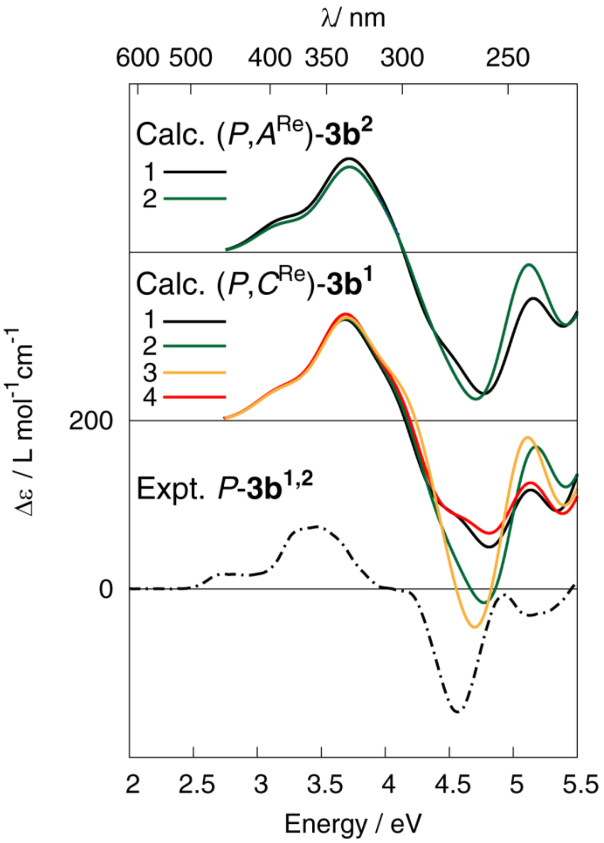

Figure S9. Comparison of the experimental (dashed line – unresolved mixture of (*P*,*C*^{Re})-**3b^1** and (*P*,*A*^{Re})-**3b^2**, DCM solvent) and TDDFT BHLYP/SV(P)/COSMO(DCM) (solid lines) CD spectra of helicene-bipyridine-rhenium complexes, (*P*,*C*^{Re})-**3b^1** and (*P*,*A*^{Re})-**3b^2**. No spectral shift has been applied. Numbers listed (1, 2, 3, 4) correspond to different conformers examined (compare Figure S8).

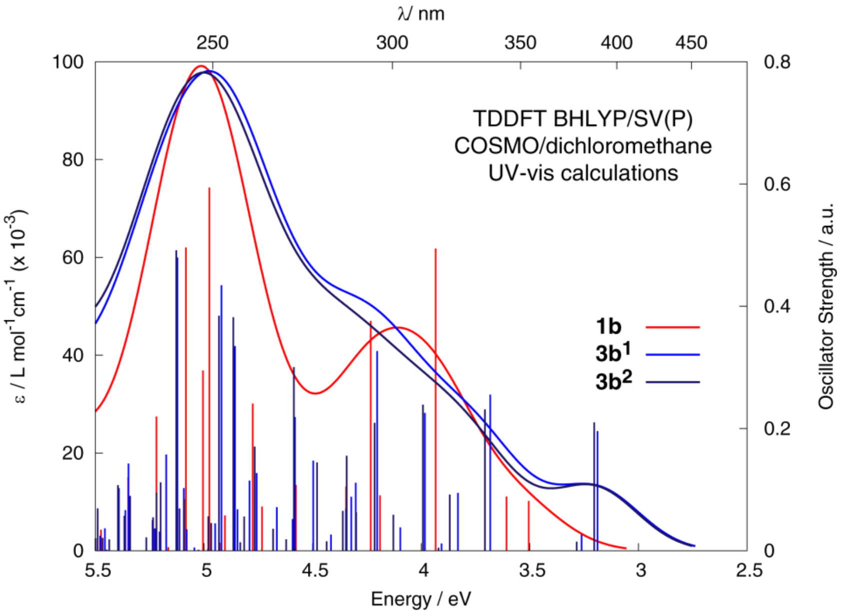

Figure S10. Comparison of the simulated (BHLYP/SV(P)/COSMO(DCM)) UV-vis spectra of **1b** (red line), **3b^1** (light blue line, conformer #1 in Figure S8), and **3b^2** (dark blue line, conformer #1 in Figure S8). No spectral shift has been applied. Calculated excitation energies and oscillator strengths indicated as 'stick' spectra.

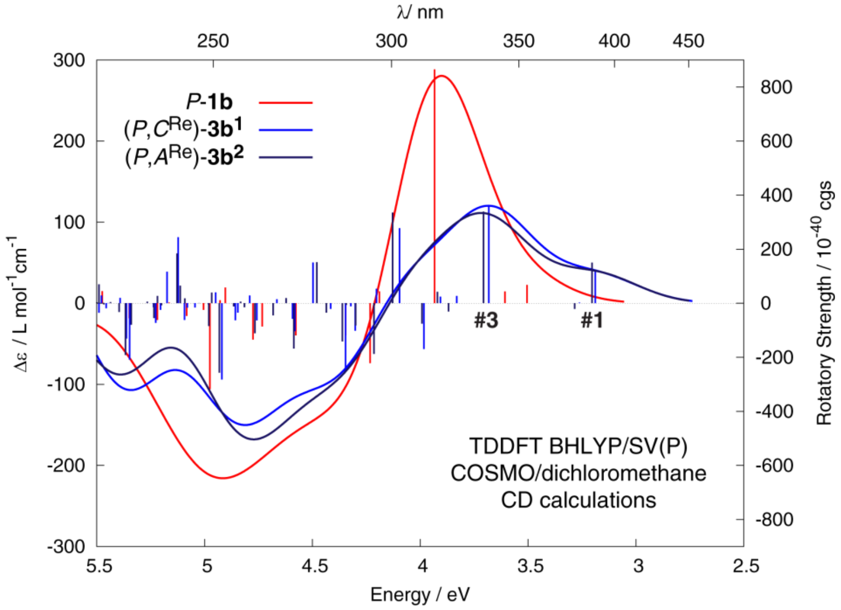

Figure S11. Comparison of the simulated (BHLYP/SV(P)/COSMO(DCM)) CD spectra of *P*-**1b** (red line), (*P*,*C*$^{\mathrm{Re}}$)-**3b^1** (light blue line, conformer #1 in Figure S8), and (*P*,*A*$^{\mathrm{Re}}$)-**3b^2** (dark blue line, conformer #1 in Figure S8). No spectral shift has been applied. Calculated excitation energies and rotatory strengths indicated as 'stick' spectra. Numbered excitations correspond to those analyzed in detail. For assignment of the CD spectrum for *P*-**1b** see ref. 1f.

Table S4. Selected dominant excitations and occupied (occ) – unoccupied (unocc) MO pair contributions (greater than 10%) of (*P*,*C*$^{\mathrm{Re}}$)-**3b^{1}** and (*P*,*A*$^{\mathrm{Re}}$)-**3b^{2}**. BHLYP/SV(P)/COSMO(DCM) calculations.

Excitation	*E* / eV	λ / nm	*f*	*R* / 10^{-40} cgs	occ no.	unocc no.	%
				3b^{1}			
#1	3.19	389	0.1957	124.39	169	170	76.7
#3	3.68	337	0.2554	358.25	169	171	50.2
					168	171	23.3
				3b^{2}			
#1	3.20	387	0.2101	150.39	169	170	74.1
#3	3.71	335	0.2313	339.06	169	171	46.3
					168	171	22.5

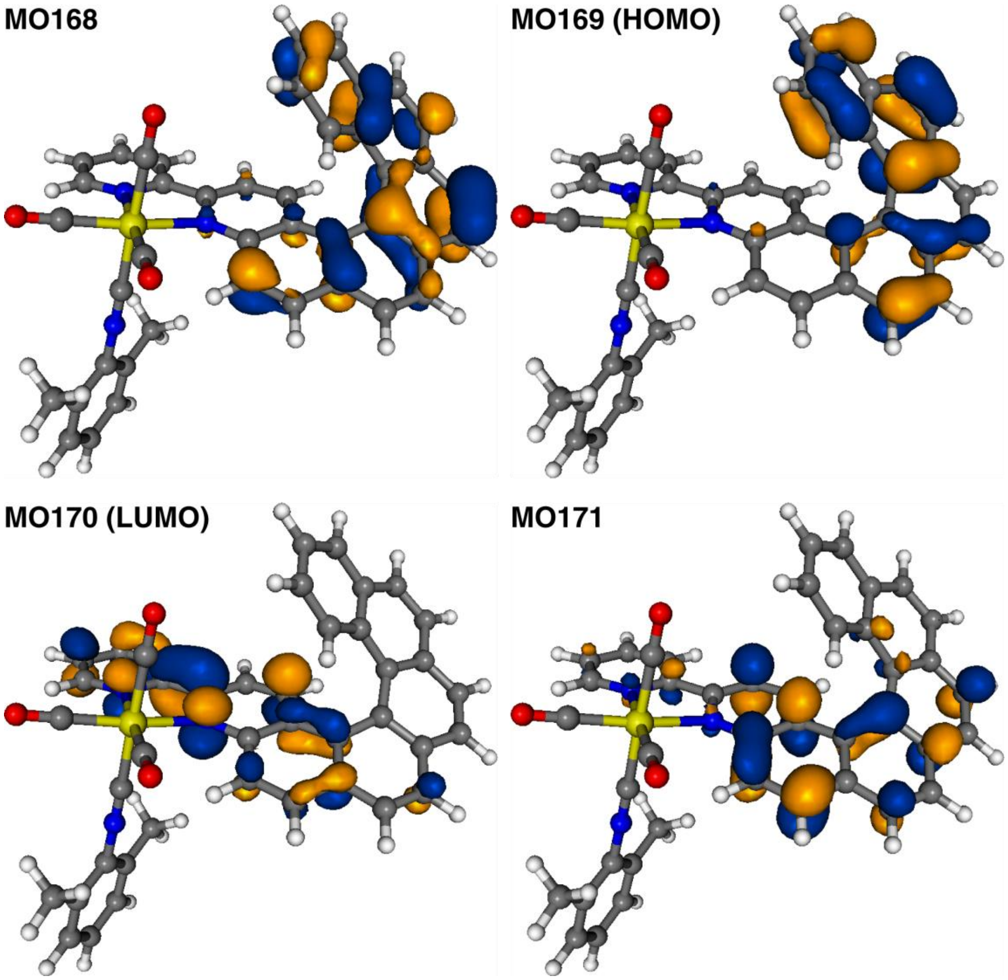

Figure S12. Isosurfaces (0.04 au) of MOs involved in selected transitions of **3b^{1}**. BHLYP/SV(P)/COSMO(DCM) calculations.

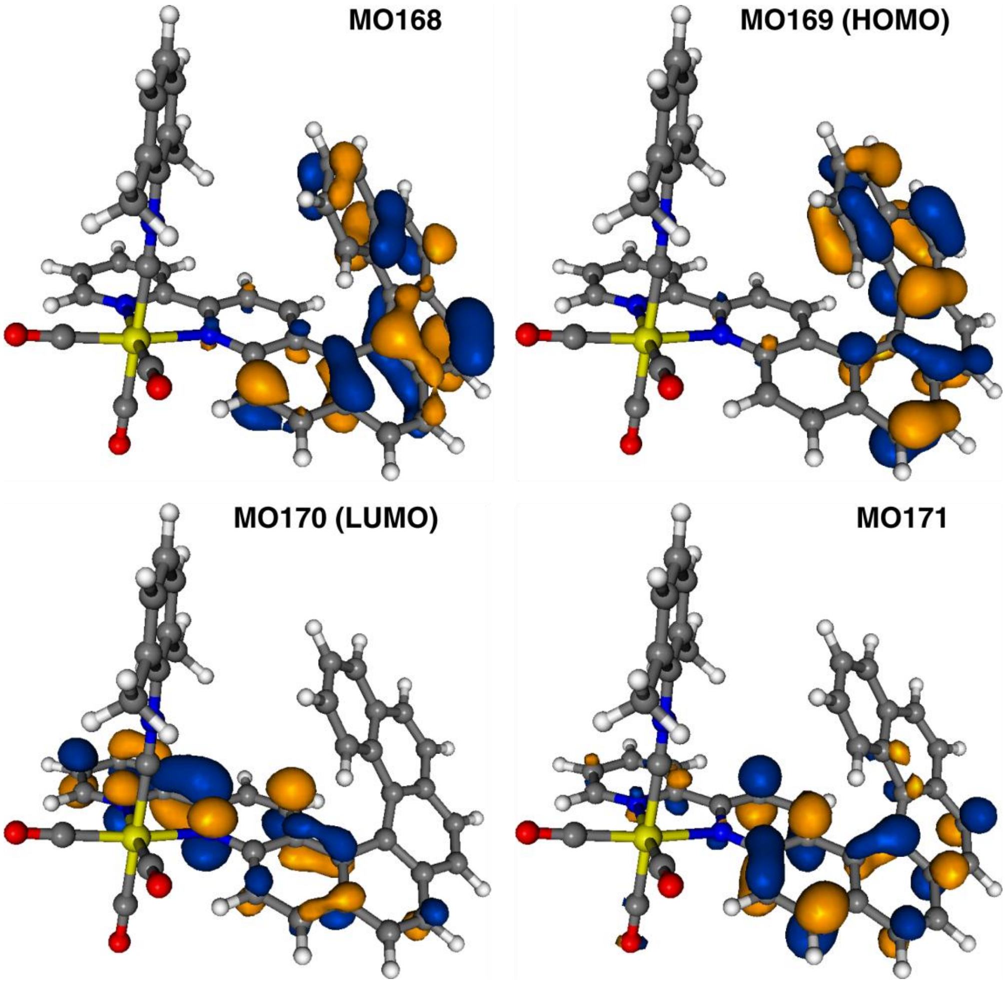

MO168

MO169 (HOMO)

MO170 (LUMO)

MO171

Figure S13. Isosurfaces (0.04 au) of MOs involved in selected transitions of **3b^2**. BHLYP/SV(P)/COSMO(DCM) calculations.

Table S5. Experimental and calculated emission data of helicene-bipyridine-rhenium complexes, **2b**^{1,2} and **3b**^{1,2}. Energies, in eV.

	(P,C^{Re})-**2b**^{1}	(P,A^{Re})-**2b**^{2}	(P,C^{Re})-**3b**^{1} [a]	(P,A^{Re})-**3b**^{2} [a]
Expt. [b]				
298 K	1.82	1.84	2.07 [c]	
77 K	2.21, 2.05, 1.90sh	2.24, 2.06, 1.90sh	2.21, 2.04, 1.88 [c]	
Calc. BHLYP/SV(P)/COSMO(DCM) [d]				
$S_1^{\{\mathrm{TDDFT}\}}$ [e]	2.38 [i] (0.0005)	2.85 (0.3791)	2.74 (0.3595)	2.75 (0.3670)
$T_1^{\{\mathrm{TDDFT}\}}$ [f]	2.14	2.16	2.09	2.09
$T_1^{\{\mathrm{DFT}\}}$ [g]	2.10	2.15	2.04	2.04
$T_1//T_1^{\{\mathrm{DFT}\}}$-$S_0//T_1^{\{\mathrm{DFT}\}}$ [h]	2.11	2.25	1.97	1.97

[a] Excited-state optimization based on the lowest-energy conformer, compare Figure S8. [b] 298 K: recorded in dichloromethane, 77 K: recorded in diethyl ether / isopentane / ethanol. [c] Data for unresolved mixture of (P,C^{Re})-**3b**^{1} and (P,A^{Re})-**3b**^{2}. [d] Dichloromethane (DCM) calculations. [e] TDDFT S_1-S_0 energy difference at TDDFT BHLYP/SV(P) optimized S_1 geometry. In parentheses oscillator strength values are listed. [f] TDDFT-TDA T_1-S_0 energy difference at TDDFT-TDA BHLYP/SV(P) optimized T_1 geometry. [g] TDDFT-TDA T_1-S_0 energy difference at DFT BP/SV(P) optimized triplet configuration. [h] DFT BHLYP/SV(P) T_1-S_0 energy gap. [i] The optimized S_1 excited state reveals different character than for the other complexes (MLCT instead of ILCT). Its low oscillator strength coincides with low oscillator strengths of absorption excitations of MLCT character computed for these systems.

Table S6. Calculated TDDFT-TDA BHLYP COSMO(DCM) spin-orbit coupling emission data of helicene-bipyridine-rhenium complexes, **2b**^{1,2} and **3b**^{1,2}. [a]

Method	$T_1^{\{TDDFT\}}$ / eV [c]	ZFS / cm^{-1} [d]		τ_i / s [e]			τ_{av} / µs [f]
		ΔE_{2-1}	ΔE_{3-1}	τ_1	τ_2	τ_3	
(*P*,*C*^{Re})-**2b**^{1}							
pSOC	2.17	0.00	0.08	9.71E-04	1.18E-0.3	3.61E-04	646
SOC	2.15	0.08	0.32	2.91E-03	6.49E-04	1.32E-04	317
Exp.							47
(*P*,*A*^{Re})-**2b**^{2}							
pSOC	2.19	0.08	0.08	2.39E-03	3.37E-03	6.07E-04	1 270
SOC	2.17	0.08	0.16	1.68E-02	1.06E-02	1.67E-04	489
Exp.							43
(*P*,*C*^{Re})-**3b**^{1}							
pSOC	2.12	0.00	0.00	1.49E-03	1.32E-03	3.87E-03	2 129
SOC	2.10	0.08	0.08	1.71E-02	3.66E-03	4.82E-04	1 273
Exp. [b]							210
(*P*,*A*^{Re})-**3b**^{2}							
pSOC	2.11	0.08	0.08	1.62E-03	2.74E-03	1.04E-02	2 785
SOC	2.10	0.00	0.00	1.63E-02	2.54E-02	4.55E-04	1 306
Exp. [b]							210

[a] Perturbative and fully self-consistent spin-orbit coupling (pSOC and SOC) calculations with TZP basis set used for Re, DZP for Cl, O, N, C, and DZ for H at TDDFT-TDA BHLYP/SV(P)/COSMO(DCM) optimized T_1 geometry. Experimental data recorded in diethyl ether / isopentane / ethanol at 77 K. [b] Data for unresolved mixture of (*P*,*C*^{Re})-**3b**^{1} and (*P*,*A*^{Re})-**3b**^{2}. [c] TDDFT energy difference between the 1st micro-state of the T_1 triplet and the ground state S_0.Within the given precision of 0.01 eV, the energies of the three triplet components are the same. [d] Energy difference between the lowest-energy component of the triplet and component 2 and 3, respectively, due to zero-field splitting. [e] Radiative lifetimes from *i*-th micro-state (i = 1, 2, 3) of the T_1 triplet decaying to the ground state, solvent-corrected by dividing by the square of the refractive index of DCM (n = 1.42). [g] Averaged radiative lifetime calculated by use of the three individual radiative decay times τ_i and of the ZFS $\Delta E_{i\text{-}1}$ values according to eq. (2) (see Computational details) for a temperature of 77 K.

Table S7. Calculated TDDFT B3LYP COSMO(DCM) spin-orbit coupling emission data of helicene-bipyridine-rhenium complexes, **$2b^{1,2}$** and **$3b^{1,2}$**. [a]

Method	$T_{11}^{\{TDDFT\}}$ / eV [c]	ZFS / cm^{-1} [d]		τ_i / s [e]			τ_{av} / μs [f]
		ΔE_{2-1}	ΔE_{3-1}	τ_1	τ_2	τ_3	
(P,C^{Re})-**$2b^1$**							
pSOC	1.91	0.97	5.57	2.67E-02	7.31E-05	3.20E-05	69
SOC	1.91	0.89	6.69	1.14E-03	8.07E-05	8.35E-06	24
Exp.							47
(P,A^{Re})-**$2b^2$**							
pSOC	1.95	0.40	3.39	1.92E-02	3.57E-04	2.25E-05	66
SOC	1.95	0.24	3.87	4.25E-03	1.09E-03	8.96E-06	28
Exp.							43
(P,C^{Re})-**$3b^1$**							
pSOC	1.86	0.00	0.16	1.54E-02	1.13E-03	6.35E-04	1188
SOC	1.85	0.48	2.18	2.10E-02	2.14E-04	2.65E-03	586
Exp. [b]							210
(P,A^{Re})-**$3b^2$**							
pSOC	1.86	0.08	0.16	1.07E-02	4.99E-04	5.59E-04	773
SOC	1.86	0.48	2.10	1.60E-02	1.99E-04	2.83E-03	550
Exp. [b]							210

[a] Perturbative and fully self-consistent spin-orbit coupling (pSOC and SOC) calculations with TZP basis set used for Re, DZP for Cl, O, N, C, and DZ for H at TDDFT-TDA BHLYP/SV(P)/COSMO(DCM) optimized T_1 geometry. Experimental data recorded in diethyl ether / isopentane / ethanol at 77 K. [b] Data for unresolved mixture of (P,C^{Re})-**$3b^1$** and (P,A^{Re})-**$3b^2$**. [c] TDDFT energy difference between the 1st micro-state of the T_1 triplet and the ground state S_0.Within the given precision of 0.01 eV, the energies of the three triplet components are the same. [d] Energy difference between the lowest-energy component of the triplet and component 2 and 3, respectively, due to zero-field splitting. [e] Radiative lifetimes calculated for i-th micro-state (i = 1, 2, 3) of the T_1 triplet decaying to the ground state, solvent-corrected by dividing by the square of the refractive index of DCM (n = 1.42). [g] Averaged radiative lifetime calculated by use of the three individual radiative decay times τ_i and of the ZFS ΔE_{i-1} values according to eq. (2) (see Computational details) for a temperature of 77 K.

Table S8. Occupied (occ) – unoccupied (unocc) MO pair contributions (greater than 1%) for T_1-S_0 emission transitions of **2b**^{1} and **2b**^{2}. BHLYP//TZP/DZP/DZ COSMO(DCM) calculations.

occ no.	unocc no.	%
	2b^1	
173a	174a	59.4
173a	176a	8.7
169a	174a	4.7
172a	174a	4.6
167a	174a	2.9
172a	175a	2.7
168a	174a	1.0
	2b^2	
173a	174a	57.0
173a	176a	10.9
169a	174a	5.3
172a	174a	4.7
172a	175a	2.9
167a	174a	2.0
173a	175a	1.4

Table S9. Occupied (occ) – unoccupied (unocc) MO pair contributions (greater than 1%) for T_1-S_0 emission transitions of **3b**^{1} and 3**b**^{2}. BHLYP//TZP/DZP/DZ COSMO(DCM) calculations.

occ no.	unocc no.	%
	3b^1	
199a	200a	56.9
199a	202a	10.7
198a	200a	5.4
197a	200a	4.5
196a	200a	3.9
198a	201a	1.9
195a	200a	1.2
192a	200a	1.1
	3b^2	
199a	200a	57.8
199a	202a	10.4
197a	200a	6.3
198a	200a	5.0
198a	201a	1.9
196a	200a	1.6
192a	200a	1.2
199a	201a	1.2
190a	202a	1.0

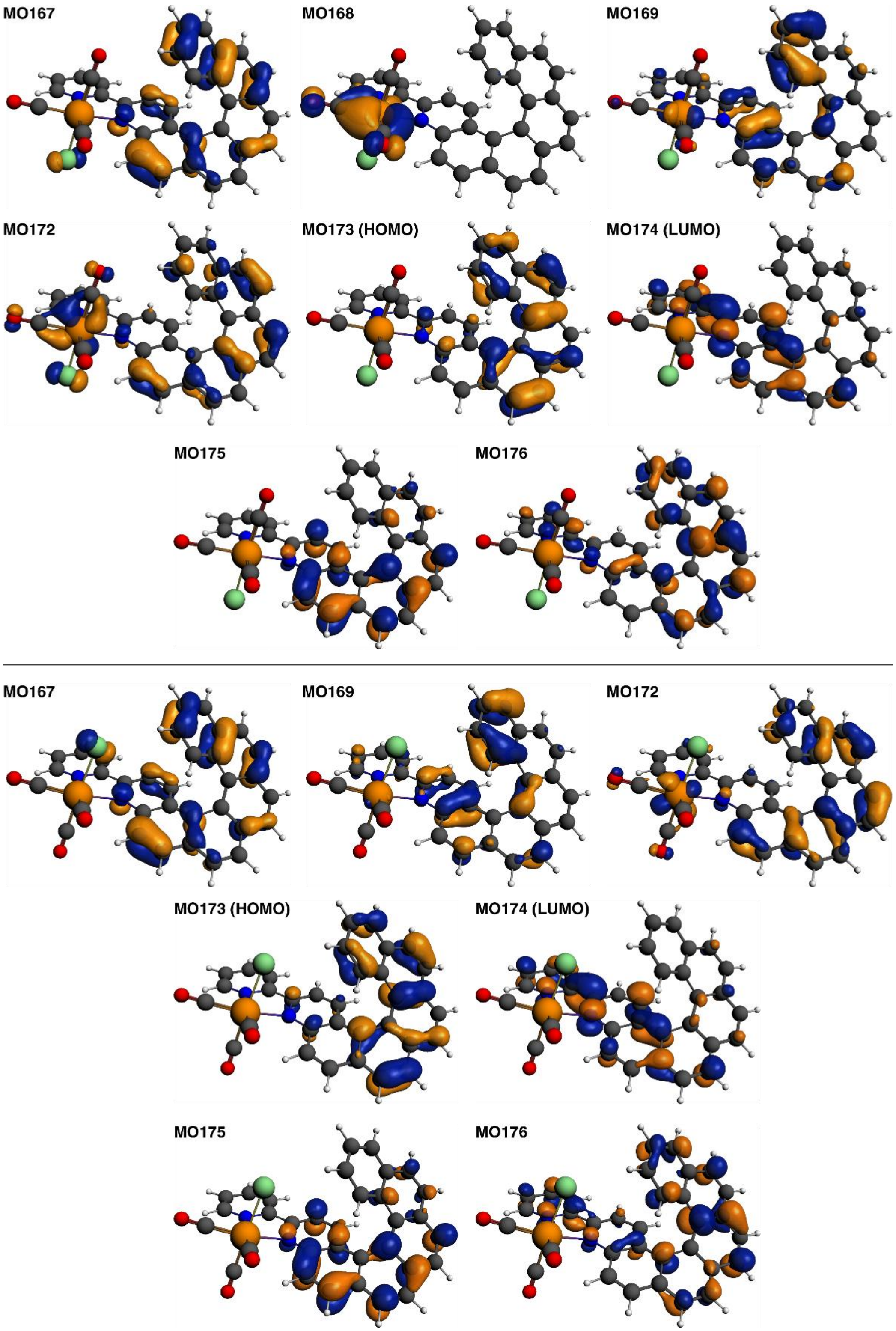

Figure S14. Isosurfaces (0.04 au) of molecular orbitals of S_0 at $T_1^{\{TDDFT\}}$ excited-state geometry involved in T_1-S_0 emission transitions of **2b^1** and **2b^2**. BHLYP//TZP/DZP/DZ COSMO(DCM) calculations. See Table S8.

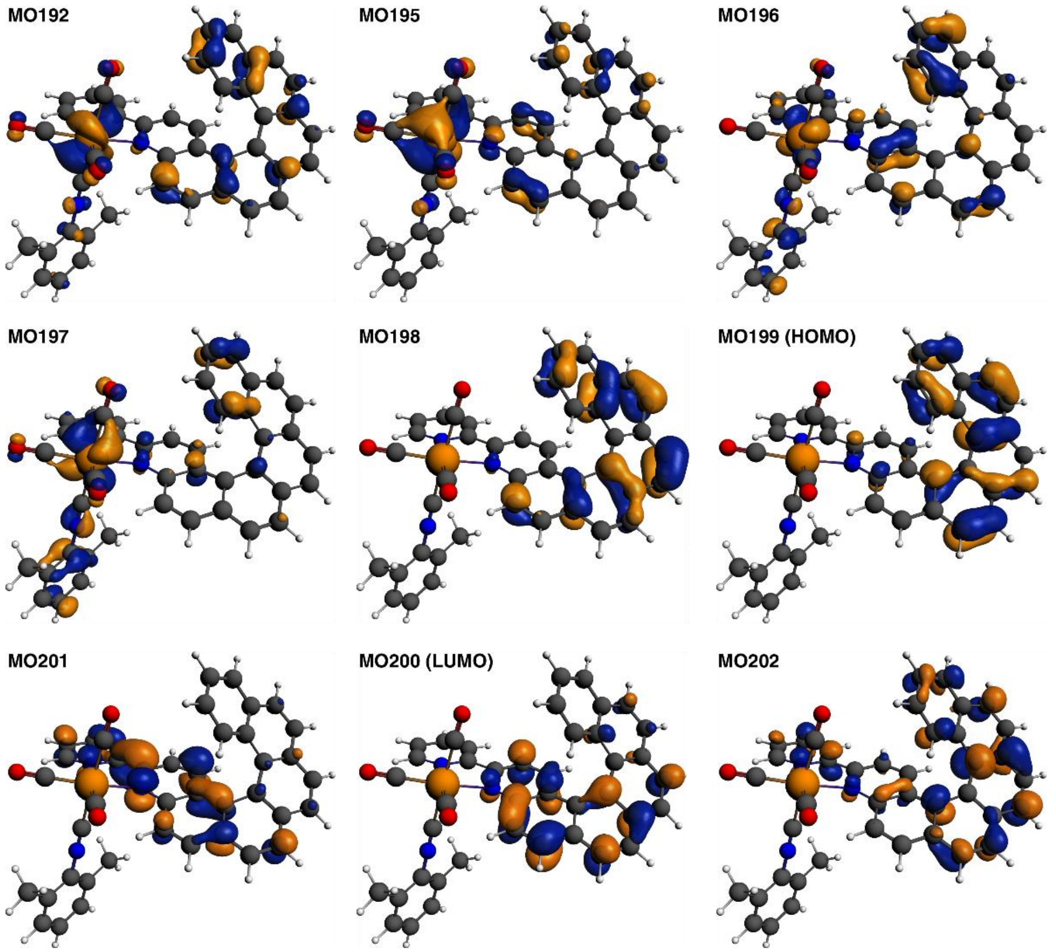

Figure S15. Isosurfaces (0.04 au) of molecular orbitals of S_0 at $T_1^{\{TDDFT\}}$ excited-state geometry involved in T_1-S_0 emission transitions of **3b^{1}**. BHLYP//TZP/DZP/DZ COSMO(DCM) calculations. See Table S9.

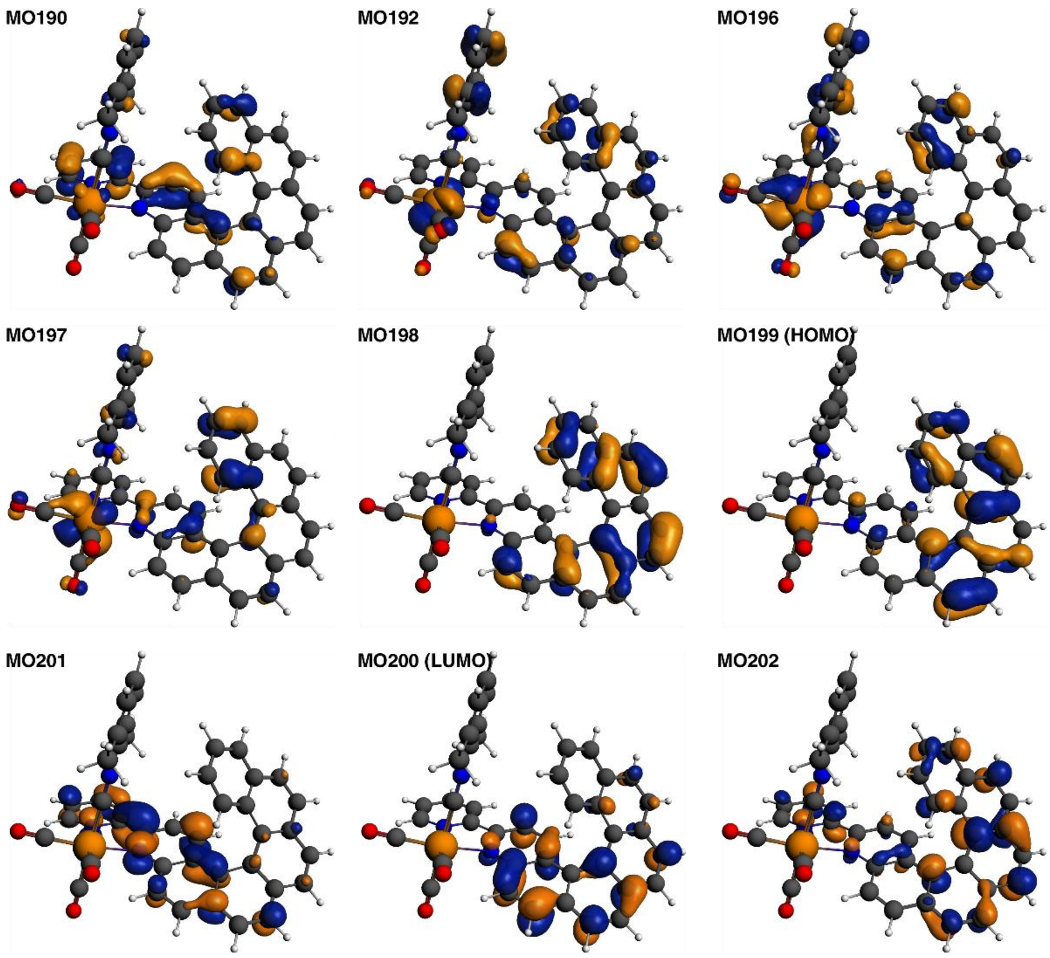

Figure S16. Isosurfaces (0.04 au) of molecular orbitals of S_0 at $T_1^{\{TDDFT\}}$ excited-state geometry involved in T_1-S_0 emission transitions of **3b**^{2}. BHLYP//TZP/DZP/DZ COSMO(DCM) calculations. See Table S9.

Table S10. Occupied (occ) – unoccupied (unocc) MO pair contributions (greater than 1%) for T_1-S_0 emission transitions of **2b**^{1} and **2b**^{2}. B3LYP//TZP/DZP/DZ COSMO(DCM) calculations.

occ no.	unocc no.	%
	2b^1	
173	174	63.7
172	174	15.1
168	174	4.9
172	176	3.1
170	174	2.4
167	174	1.7
170	175	1.3
173	176	1.3
	2b^2	
173	174	65.0
172	174	8.4
168	174	5.0
173	176	4.0
170	174	4.0
172	176	3.0
170	175	1.5
171	174	1.3
167	174	1.1

Table S11. Occupied (occ) – unoccupied (unocc) MO pair contributions (greater than 1%) for T_1-S_0 emission transitions of **3b**^{1} and 3**b**^{2}. B3LYP//TZP/DZP/DZ COSMO(DCM) calculations.

occ no.	unocc no.	%
	3b^1	
199	200	75.9
199	202	5.9
196	200	5.1
198	200	4.6
197	200	1.2
	3b^2	
199a	200a	76.0
199a	202a	6.0
198a	200a	4.4
196a	200a	3.5
197a	200a	1.6
195a	200a	1.1

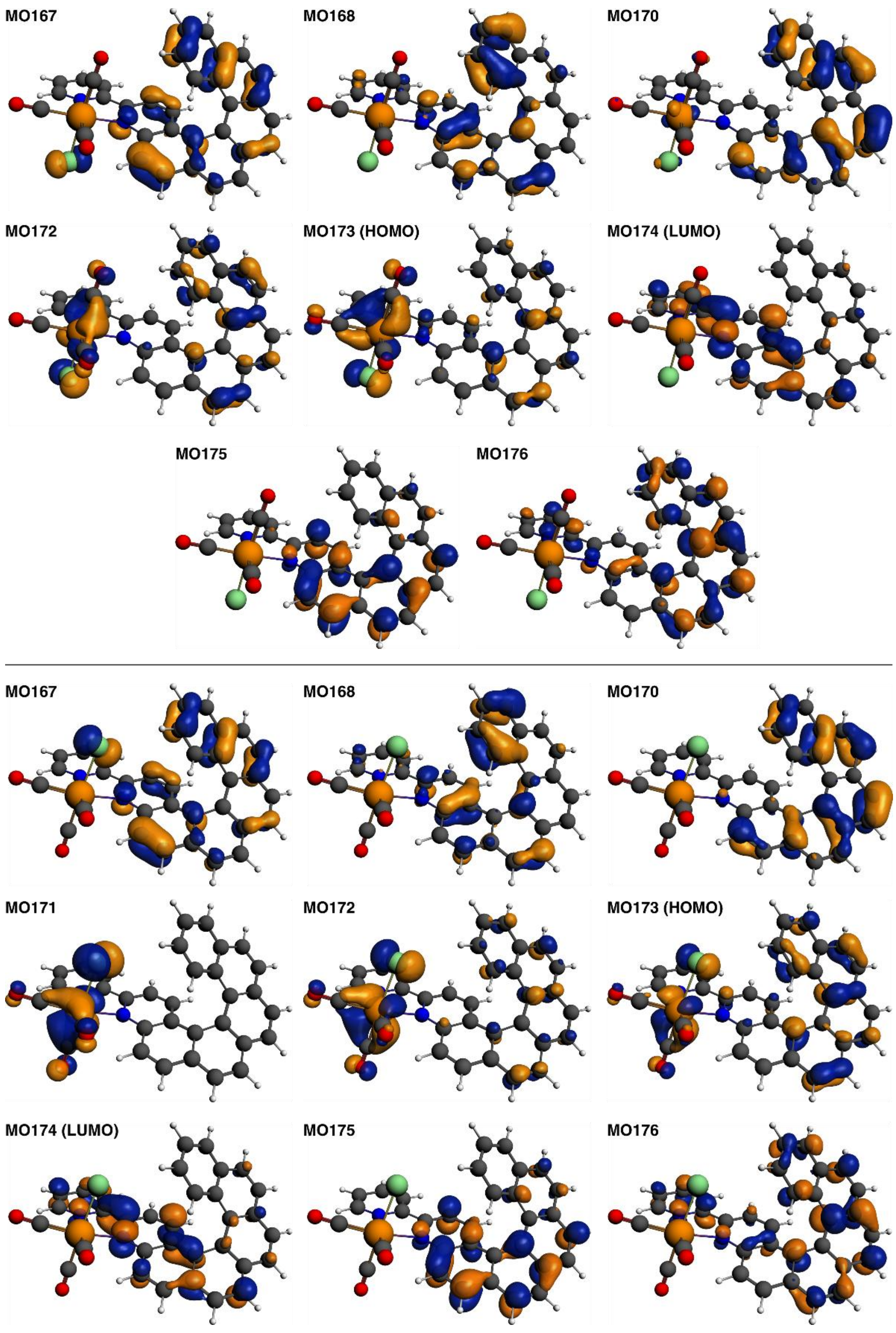

Figure S17. Isosurfaces (0.04 au) of molecular orbitals of S_0 at $T_1^{\{TDDFT\}}$ excited-state geometry involved in T_1-S_0 emission transitions of $\mathbf{2b^1}$ and $\mathbf{2b^2}$. B3LYP//TZP/DZP/DZ COSMO(DCM) calculations. See Table S10.

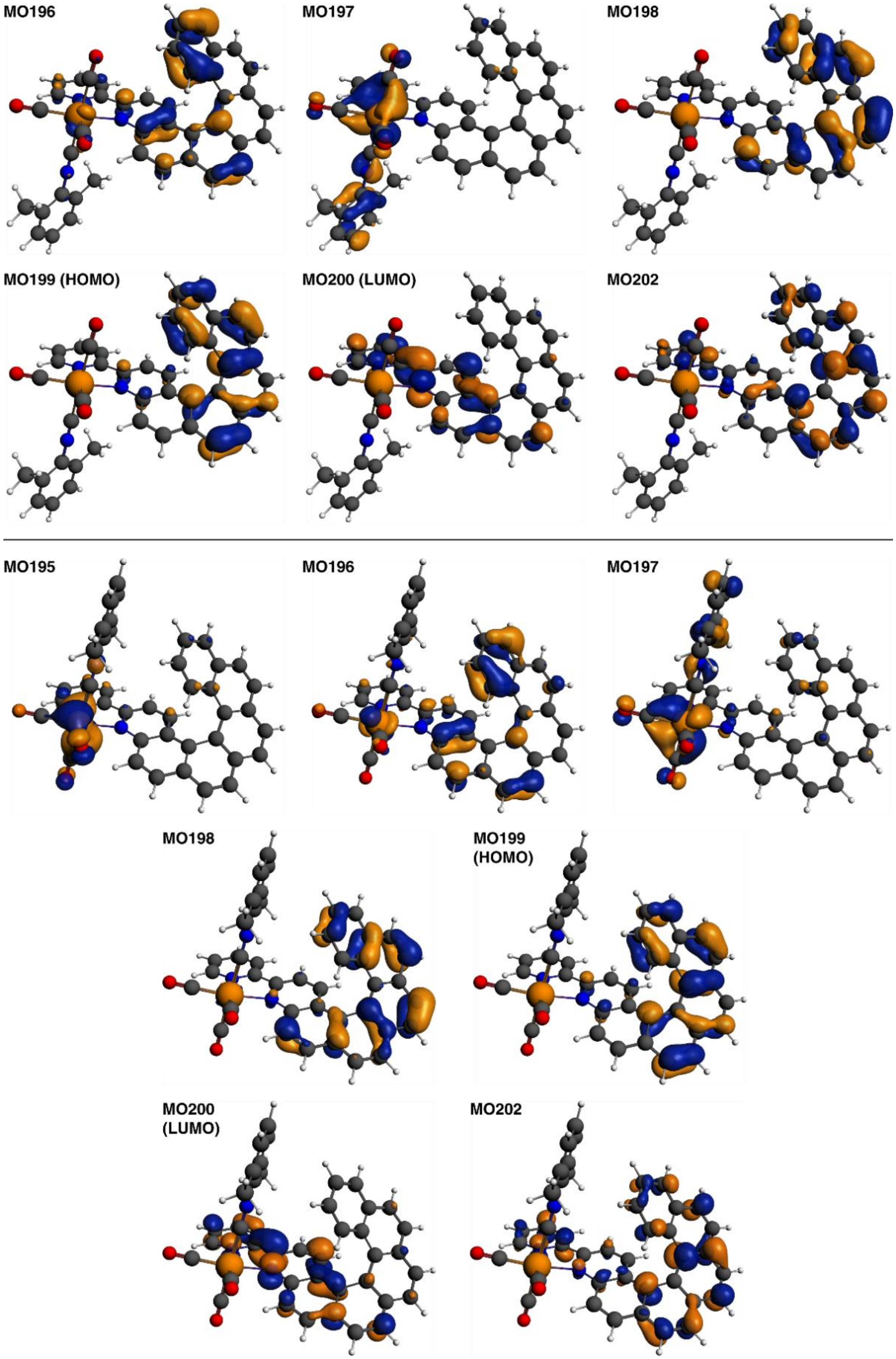

Figure S18. Isosurfaces (0.04 au) of molecular orbitals of S_0 at $T_1^{\{TDDFT\}}$ excited-state geometry involved in T_1-S_0 emission transitions of 3**b**^{1} and **3b**^{2}. B3LYP//TZP/DZP/DZ COSMO(DCM) calculations. See Table S11.

B. Experimental part

General

All experiments were performed under an atmosphere of dry argon using standard Schlenk techniques. Commercially available reagents were used as received without further purification. Solvents were freshly distilled under argon from sodium/benzophenone (tetrahydrofuran, diethyl ether) or from phosphorus pentoxide (pentane, dichloromethane). Irradiation reactions were conducted using a Heraeus TQ 150 mercury vapor lamp. Preparative separations were performed by gravity column chromatography on basic alumina (Aldrich, Type 5016A, 150 mesh, 58 Å) or silica gel (Merck Geduran 60, 0.063-0.200 mm) in 3.5-20 cm columns. ^{1}H, ^{13} C, and ^{31} P NMR spectra were recorded on a Bruker AM300, AV400 or AV500. ^{1}H and ^{13}C NMR chemical shifts were reported in parts per million (ppm) relative to Me_4Si as external standard. ^{31}P NMR downfield chemical shifts were expressed with a positive sign, in ppm, relative to external 85% H_3PO_4 and were decoupled from the proton. Assignment of proton atoms is based on COSY experiment. Assignment of carbon atoms is based on HMBC, HMQC and DEPT-135 experiments. High-resolution mass spectra were obtained on a Varian MAT 311 or ZabSpec TOF Micromass instrument at CRMPO, University of Rennes 1. Elemental analyses were performed by the CRMPO, University of Rennes 1. UV-vis spectroscopy was conducted on a Varian Cary 5000 spectrometer. Specific rotations (in deg cm^2 g^{-1}) were measured in a 1 dm thermostated quartz cell on a Perkin Elmer-341 polarimeter. Circular dichroism (in M^{-1} cm^{-1}) was measured on a Jasco J-815 Circular Dichroism Spectrometer (IFR140 facility - Biosit platform - Université de Rennes 1). Ligands **1a** and enantiopure *M*- and *P*-**1b** were prepared according to the litterature.[18]

Complex (±)-2a

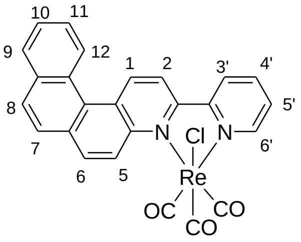

3-(2-Pyridyl)-4-aza[4]-helicene **1a** (42.5 mg, 0.138 mmol) and $Re(CO)_5Cl$ (50.2 mg, 0.138 mmol) of were refluxed in distillated toluene (3 mL) under argon atmosphere for 5 hours during which an orange solid precipitated. The reaction mixture was then cooled to room temperature and the solid was filtered off and washed with pentane and ether, providing (±)-**2a** (76 mg, 90%) as an orange powder.

^{1}H NMR (400 MHz, CD_2Cl_2): δ 9.61 (1 H, d, J = 9 Hz, H^{1}), 9.14(1 H, ddd, J = 5.6, 4.8, 0.8 Hz, $H^{6'}$), 8.90 (1 H, d, J = 9.3 Hz, H^{5}), 8.77 (1 H, d, J = 8.1 Hz, H^{12}), 8.38 (1 H, d, J = 8.1 Hz, $H^{3'}$), 8.32 (1 H, d, J = 9.3 Hz, H^{2}), 8.27 (1 H, d, J = 9.3 Hz, H^{6}), 8.02 - 8.15 (3 H, m, $H^{4',9,7}$), 7.90 (1 H, d, J = 8.7 Hz, H^{8}), 7.66 - 7.77 (2 H, m, $H^{10,11}$), 7.55 (1 H, ddd, J = 7.6, 5.5, 1.3 Hz, $H^{5'}$). ^{13}C NMR (101 MHz CD_2Cl_2): δ 160.39 (*C*), 157.82 (*C*), 153.59 (*CH*), 149.67 (*C*), 139.93 (*CH*), 139.55 (*CH*), 134.51 (*C*), 134.19 (*CH*), 132.35 (*C*), 130.70 (*C*), 130.63 (*CH*), 129.97 (*C*), 129.85 (*CH*), 129.59 (*CH*), 128.00 (*CH*), 127.95 (*C*), 127.80 (*CH*), 127.70 (*CH*), 127.31 (*CH*), 126.61 (*CH*), 124.86 (*CH*), 118.59 (*CH*). 3 *C*O not seen. Elemental analysis, calcd. (%) for $C_{25}H_{14}ClN_2O_3Re$: C, 49.06; H, 2.31; found C 48.97, H 1.98.

Complex (±)-3a

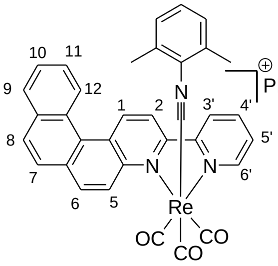

Complex (±)-**2a** (53 mg, 0.087 mmol) and AgOTf (22.3 mg, 0.087 mmol) were dissolved in an ethanol (25 mL) / THF (10 mL) mixture and refluxed in the dark for 6 hours. The solution was then filtered over celite and the THF was concentrated *in vacuo*. Then a solution of 2,6-dimethylphenyl isocyanide (11.3 mg, 0.087 mmol) in ethanol (2 mL) was added and the reaction mixture was refluxed overnight and under argon atmosphere. The ethanol solvent was evaporated to a small volume (c.a. 3~4 mL) then 7 ml of saturated NH_4PF_6 aq. solution was added. A yellow precipitate directly was observed and was isolated by vacuum filtration, washed with water, pentane, and ether, then dried at 50 ºC for several hours leading (±)-**3a** (59 mg, 80 %) as an orange powder. ^1H NMR (400 MHz, CD_2Cl_2): δ 9.78 (1 H, d, *J* = 9.3 Hz, H^1), 9.17 (1 H, dd, *J* = 5.6, 0.8 Hz, $H^{6'}$), 8.78 (1 H, d, *J* = 8.4 Hz, H^{12}), 8.72 (1 H, d, *J* = 8.1 Hz, $H^{3'}$), 8.69 (1 H, d, *J* = 9 Hz, H^5), 8.62 (1 H, d, *J* = 9 Hz, H^2), 8.30 - 8.39 (2 H, m, $H^{4',6}$), 8.05 - 8.11 (2 H, m, $H^{7,9}$), 7.92 (1 H, d, *J* = 8.7 Hz, H^8), 7.78 - 7.85 (1 H, m, H^{11}), 7.68 - 7.76 (2 H, m, $H^{10,5'}$), 7.07 (1 H, t, *J* = 7.6 Hz, $H_{isocyanide}$), 6.92 (2 H, d, *J* = 7.6 Hz, $H_{isocyanide}$), 1.89 (6 H, s, $H_{Me(isocyanide)}$). ^{13}C NMR (101 MHz, $CDCl_3$): δ 191.80 (*C*O), 191.35 (*C*O), 188.57 (*C*O), 157.91 (*C*), 156.34 (*C*), 154.12 (*C*), 154.07 (*C*H), 150.13 (*C*), 141.78 (*C*H), 141.73 (*C*H), 136.03 (*C*), 135.93 (*C*), 135.37 (*C*), 135.32 (*C*H), 134.62 (*C*), 132.44 (*C*), 131.48 (*C*H), 130.85 (*C*H), 129.79 (*C*), 129.68 (*C*H), 128.99 (*C*H), 128.79 (*C*), 128.73 (*C*H), 128.63 (*C*H), 128.56 (2*C*H), 128.28 (*C*H), 127.69 (*C*H), 126.95 (*C*), 126.62 (*C*H), 126.29 (*C*H), 119.57 (*C*H), 18.33 (2CH_3). Elemental analysis, calcd. (%) for $C_{34}H_{23}F_6N_3O_3PRe$: C, 47.89; H, 2.72; found C 47.79, H 2.72.

Complex (±)-4a

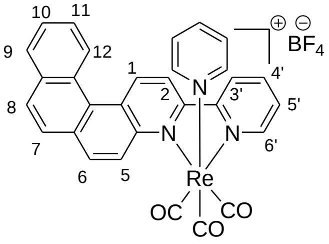

To a solution of (±)-**2a** (63 mg, 0.103 mmol) in acetonitrile (20 ml) was added $AgBF_4$ (20 mg, 0.103 mmol). The mixture was heated at reflux overnight in the dark and under argon atmosphere. The solution mixture was then filtrated over celite to remove AgCl salt and the solvent was stripped off *in vacuo* leading [(**1a**)Re$(CO)_3NCCH_3$]BF_4. Then THF (15 mL) and pyridine (25 µL, 0.31 mmol) were added and the mixture was heated at 50°C for 20 hours. The resultant solution was subsequently filtered through celite prior to the removal of the solvent *in vacuo* to furnish (±)-**4a** (61 mg, 80%) as an orange precipitate. ^1H NMR (400 MHz, CD_2Cl_2): δ 9.76 (1 H, d, *J*=9.3 Hz, H^1), 9.25 (1 H, m, $H^{6'}$), 8.84 (1 H, d, *J*=9.3 Hz, H^5), 8.78 (1 H, d, *J* = 8.4 Hz, H^{12}), 8.64 (1 H, d, *J* = 8.1 Hz, $H^{3'}$), 8.52 (1 H, d, *J* = 9.3 Hz, H^2), 8.40 (1 H, dd, *J* = 9.3 Hz, H^6), 8.29 - 8.37 (1 H, m, $H^{4'}$), 8.06 - 8.15 (2 H, m, $H^{9,7}$), 7.95(1 H, d, *J* = 8.7 Hz, H^8), 7.66 - 7.81 (6 H, m, $H^{5',11,12,py}$), 7.05 -

7.13 (2 H, m, H^{py}). ^{13}C NMR (101 MHz CD_2Cl_2): δ 196.50 (*CO*), 195.26 (*CO*), 191.71 (*CO*), 157.38 (*C*), 156.07 (*C*), 153.39 (*C*H), 151.88 (2*C*H), 149.24 (*C*), 142.17 (*C*H), 141.98 (*C*H), 140.33 (*C*H), 135.83 (*C*H), 134.64 (*C*), 132.51 (*C*), 131.52 (*C*H), 129.81 (*C*), 129.67 (*C*H), 129.33 (*C*H), 128.87 (*C*), 128.69 (*C*H), 128.30 (2*C*H), 128.27 (*C*H), 127.82 (*C*H), 127.37 (*C*H), 127.16 (*C*), 127.03 (*C*H), 126.35 (*C*H), 120.06 (*C*H). Elemental analysis, calcd. (%) for $C_{30}H_{19}BF_4N_3O_3Re$: C, 48.53; H, 2.58; found C 48.42, H 2.52.

Racemic and enantiopure complexes *M*-(-) and *P*-(+)-2b^{1,2}

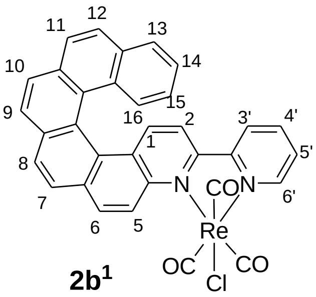

2b^1

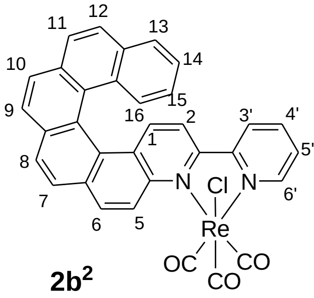

2b^2

3-(2-Pyridyl)-4-aza[6]helicene (±)-**1b** (30 mg, 0.0738 mmol) and $Re(CO)_5Cl$ (27 mg, 0.0246 mmol) were heated to reflux in 2 mL distilled toluene for 5 hours. Toluene was evaporated under reduced pressure and the mixture was purified over silica gel column chromatography (heptane/ethyl acetate 4:6 as the eluent) to provide two different Re complexes (M^*,A^{Re^*})-**2b^1** (**F2**) (14.4 mg, 28%) and (M^*,C^{Re^*})-**2b^2** (**F1**) (27.2 mg, 52%) as red orange solids. Single crystals of complex (M^*,C^{Re^*})-**2b^2** were grown by slow evaporation of a CH_2Cl_2 solution. Elemental analysis, calcd. (%) for $C_{33}H_{18}ClN_2O_3Re$: C, 55.65; H, 2.55; found C 55.46, H 2.68.

The same procedure applied to *M*-(-)-**1b** yielded respectively (M,A^{Re})-(-)-**2b^1** and (M,C^{Re})-(-)-**2b^2** , while *P*-(-)-**1b** gave respectively (P,C^{Re})-(+)-**2b^1** and (P,A^{Re})-(+)-**2b^2**. Specific and molar rotations: (P,C^{Re})-**2b^1**: $[\alpha]_D^{23}$ = 1440; $[\phi]_D^{23}$= 10250 (± 5%); (P,A^{Re})-**2b^2**: $[\alpha]_D^{23}$ = 1200;$[\phi]_D^{23}$= 8550 (± 5%); (M,A^{Re})-**2b^1**: $[\alpha]_D^{23}$ = -1440; $[\phi]_D^{23}$= -10250 (± 5%); (M,C^{Re})-**2b^2**: $[\alpha]_D^{23}$ = -1100;$[\phi]_D^{23}$= 7840 (± 5%) ($C = 5 \times 10^{-5}$ M, CH_2Cl_2).

(±)-2b^1. ^{1}H NMR (400 MHz, CD_2Cl_2): δ 9.06 (1 H, m, $H^{6'}$), 8.91 (1 H, d, *J*=9.3 Hz, H^1), 8.36 (1 H, d, *J* = 9.3 Hz, H^2), 8.18 (1 H dd, *J*=8.8, 1 Hz), 8.15 (1 H, d, *J*=8.4 Hz), 8.03 - 8.06 (3 H, m), 7.89 - 7.98 (4 H, m), 7.78 - 7.82 (1 H, m, H^{13}), 7.51 - 7.55 (1 H, m, H^{16}), 7.46 - 7.51 (1 H, m, $H^{5'}$), 7.29 (1 H, d, *J*=9 Hz), 7.14 (1 H, ddd, *J*=8.1, 6.9, 1.3 Hz, H^{14}), 6.73 (1 H, ddd, *J*=8.5, 6.9, 1.4 Hz, H^{15}). ^{13}C NMR (75 MHz, CD_2Cl_2): δ 198.03 (*C*O), 197.49 (*C*O), 189.52 (*C*O), 157.14 (*C*), 155.27 (*C*), 153.32 (*C*H), 148.34 (*C*), 139.43 (*C*H), 138.71 (*C*H), 134.33 (*C*), 133.88 (*C*H), 132.81 (*C*), 132.48 (*C*), 132.18 (*C*), 130.12 (*C*H), 129.80 (*C*H), 129.04 (*C*H), 128.99 (*C*H), 128.94 (*C*), 128.51 (*C*H), 128.07 (*C*H), 127.79 (*C*), 127.71 (*C*H), 127.40 (*C*H), 127.33 (*C*H), 126.77 (*C*), 126.68 (*C*H), 126.52 (*C*H), 125.82 (*C*H), 124.38 (*C*H), 124.10 (*C*), 116.89 (*C*H) One *C* not seen.

(±)-2b^2. ^{1}H NMR (400 MHz, CD_2Cl_2): δ 9.06 (1 H, m, $H^{6'}$), 8.84 (1 H, d, *J* = 9 Hz, H^1), 8.33 (1 H, d, *J* = 9 Hz, H^2), 8.13 - 8.20 (2 H, m), 8.01 - 8.08 (3 H, m), 7.92 - 7.96 (2 H, m, $H^{4'}$, $H^{3'}$), 7.89 (2 H, s), 7.71 - 7.79 (1 H, m, H^{13}), 7.56 (1 H, d, *J*=8.70 Hz, H^{16}), 7.36 - 7.48 (1 H, m, $H^{5'}$), 7.26 (1 H, d, *J*=9.26 Hz), 7.17 (1 H, ddd, *J* = 8.13, 7.01, 1.12 Hz, H^{14}), 6.92 (1 H, ddd, *J* = 8.41, 7.01, 1.40 Hz, H^{15}). ^{13}C NMR (75 MHz, CD_2Cl_2): δ 198.30 (*C*O), 197.87 (*C*O), 190.40 (*C*O), 171.19 (s, 1 C), 157.53 (s, 1 C), 155.72 (s, 1 C), 153.27 (*C*H), 148.14 (s, 1 C), 139.42 (*C*H), 138.79 (*C*H), 134.47 (s, 1 C), 133.89 (*C*H), 132.59 (s, 1 C), 132.55 (s, 1 C), 130.21 (*C*H), 130.03 (*C*H), 129.21 (*C*H), 129.08 (*C*H), 128.76 (s, 1 C), 128.33 (*C*H), 128.27 (*C*H), 127.66 (*C*H), 127.51 (s, 1 C), 127.37 (*C*H), 127.00 (*C*H), 126.92 (*C*H), 126.89 (s, 1 C), 126.70 (*C*H), 126.39 (*C*H), 124.60 (*C*H), 124.38 (s, 1 C), 116.86 (*C*H)

Diastereomeric mixture 3b^{1,2}

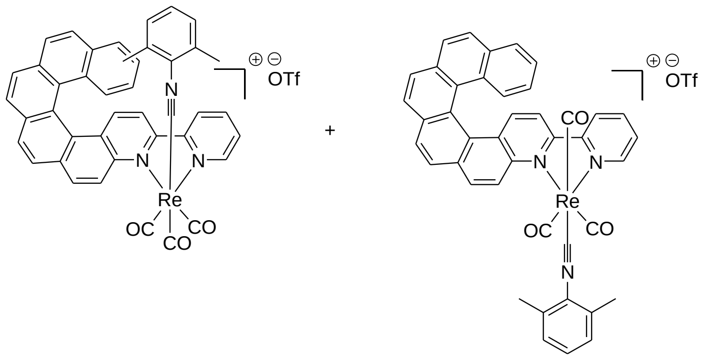

A solution of 60 mg (0.084 mmol) of **2b^{1,2}** and AgOTf (22 mg, 0.084 mmol) in ethanol / THF (25:10 mL) mixture is refluxed in the dark for 6 hours. The solution was then filtered over celite prior to the removal of THF solvent under vacuum. Then a solution of 2,6-dimethylphenyl isocyanide (11.3 mg, 0.087 mmol) in ethanol (5 mL) was added to the reaction mixture which was refluxed overnight. The ethanol stripped off and the crude mixture was purified by column chromatography over silica gel (CH_2Cl_2/acetone; from 10:0 to 7:3) to obtain **3b^{1,2}** as yellow orange powder product (60 mg, 75%) and as a mixture of two diastereomers.

^{1}H NMR (400 MHz, CD_2Cl_2) δ 9.20 - 9.25 (m, 2 H) 8.74 - 8.81 (m, 2 H) 8.52 - 8.58 (m, 3 H) 8.45 - 8.51 (m, 3 H) 8.29 - 8.41 (m, 4 H) 8.16 - 8.23 (m, 6 H) 8.03 - 8.09 (m, 4 H) 7.97 (d, *J*=7.34 Hz, 1 H) 7.75 - 7.87 (m, 4 H) 7.72 (d, *J*=8.99 Hz, 1 H) 7.64 (d, *J*=8.62 Hz, 1 H) 7.55 (d, *J*=8.25 Hz, 1 H) 7.35 - 7.41 (m, 1 H) 7.29 (ddd, *J*=7.89, 6.97, 1.10 Hz, 1 H) 7.24 (m, 2 H) 7.20 (d, *J*=7.70 Hz, 1 H) 7.06 (m, 2 H) 6.81 (ddd, *J*=8.48, 7.01, 1.38 Hz, 1 H) 6.57 (ddd, *J*=7.98, 6.97, 1.01 Hz, 1 H) 5.98 (ddd, *J*=8.44, 6.97, 1.28 Hz, 1 H) 2.07 (s, 12 H)

^{13}C NMR (101 MHz, CD_2Cl_2) δ 191.60 (*C*O) 191.48 (*C*O) 191.00 (*C*O) 190.89 (*C*O) 188.60 (*C*O) 187.83 (*C*O) 157.29 (*C*) 157.24 (*C*) 155.78 (*C*) 155.62 (*C*) 153.72 (*C*H) 153.41 (*C*H) 148.50 (*C*) 148.48 (*C*) 141.47 (*C*H) 141.33 (*C*H) 140.08 (*C*H) 139.89 (*C*H) 135.68 (*C*) 135.58 (*C*) 134.94 (*C*H) 134.76 (*C*H) 134.33 (*C*) 134.30 (*C*) 132.77 (*C*) 132.76 (*C*) 132.41 (*C*) 132.35 (*C*) 132.18 (*C*) 131.89 (*C*) 130.86 (*C*H) 130.48 (*C*H) 130.45 (*C*H) 130.40 (*C*H) 130.39 (*C*H) 129.36 (*C*H) 129.30 (*C*H) 129.17 (*C*H) 129.07 (*C*H) 128.78 (*C*) 128.72 (*C*H) 128.71 (*C*H) 128.68 (*C*H) 128.62 (*C*) 128.61 (*C*) 128.60 (*C*H) 128.56 (*C*H) 128.55 (*C*H) 128.54 (*C*H) 128.52 (*C*H) 128.43 (*C*) 128.31 (*C*) 128.30 (*C*) 128.20 (*C*H) 128.19 (*C*H) 128.16 (*C*H) 127.51 (*C*H) 127.50 (*C*H) 127.47 (*C*H) 127.34 (*C*H) 127.29 (*C*H) 126.90 (*C*H) 126.88 (*C*) 126.86 (*C*) 126.85 (*C*) 126.75 (*C*H) 126.6 (*C*) 126.59 (*C*) 126.46 (*C*H) 126.37 (*C*H) 126.36 (*C*H) 126.12 (*C*H) 125.96 (*C*H) 125.60 (*C*H) 125.25 (*C*H) 124.16 (*C*H) 123.74 (*C*) 123.68 (*C*) 122.58 (*C*) 119.39 (*C*) 117.88 (*C*H) 117.70 (*C*H) 18.20 (CH_3) 18.09 (CH_3).

The same procedure applied to *M*-(-)-**1b** and while *P*-(-)-**1b** yielded respectively (*P*,*AC*^{Re})-(+)-**3b^1** and (*M*,*AC*^{Re})-(+)-**3b^2**. Specific and molar rotations: (*P*,*AC*^{Re})-**3b^1**: $[\alpha]_D^{23}$ = 1570; $[\phi]_D^{23}$= 15040 (± 5%) (C = 8.8 × 10^{-5} M, CH_2Cl_2).; (*M*,*AC*^{Re})-**3b^2**: $[\alpha]_D^{23}$ = -1490; $[\phi]_D^{23}$ = -14230 (± 5%) (C = 9.7 × 10^{-5} M, CH_2Cl_2).

UV-vis spectra

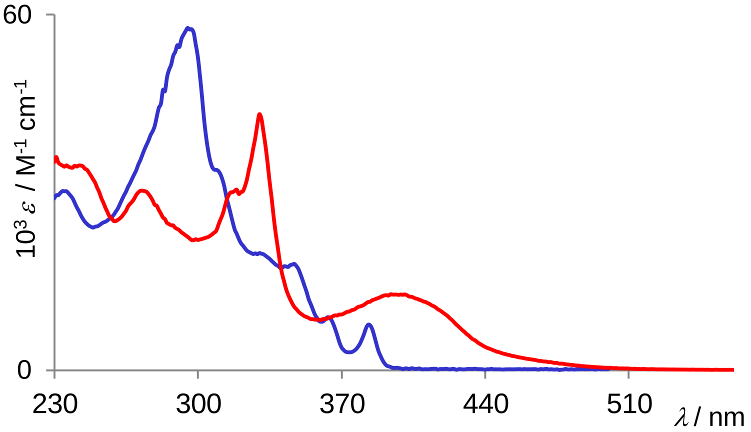

Figure S19. UV-Vis spectra of ligand **1a** (blue) and complex **2a** (red) in CH_2Cl_2 (*C* 5. 10^{-5} M).

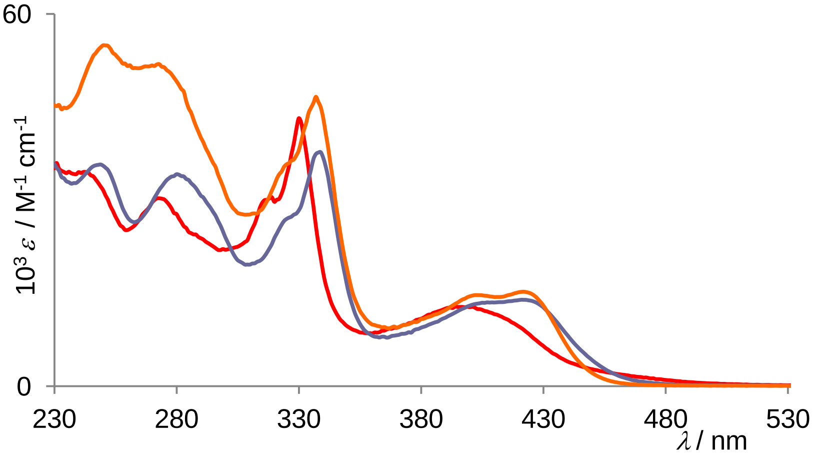

Figure S20. UV-Vis spectra of complexes **2a** (red), **3a** (orange) and **4a** (blue) in CH_2Cl_2 (*C* 5. 10^{-5} M).

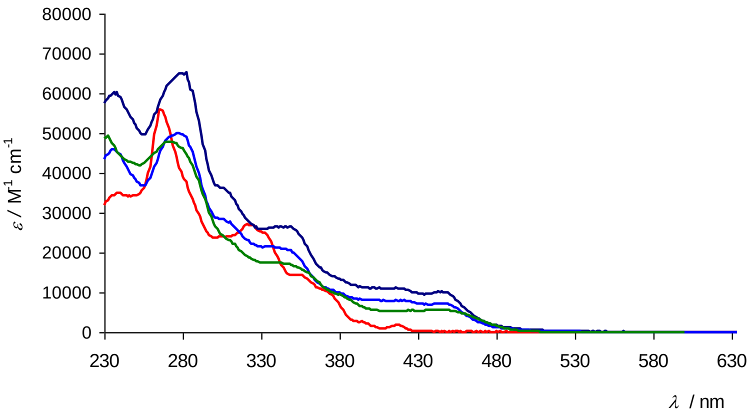

Figure S21. UV-Vis spectra of ligand **1b** (red) and complexes **2b^1** (light blue) and **2b^2** (dark blue) and **3b^{1,2}** (green) in CH_2Cl_2 (*C* 5. 10^{-5} M).

A and *C* configuration at rhenium centers

The configuration is described by the steering-wheel system, a principle put by Cahn, Ingold, and Prelog[19] consisting of an oriented plane (or circle) traversed by a vector oriented perpendicularly to the plane. The orientation in the plane or around the circle, both to the right or to the left, is unambiguous and will be called "*C*" and "*A*" (Figure S17).

The priority rules (sequence rule) allow the oriented plane and axis to be defined as *C* or *A*. The priority rules are the same in coordination chemistry as in organic chemistry.[52]

Priority 1 2 3, the oriented plane P is:

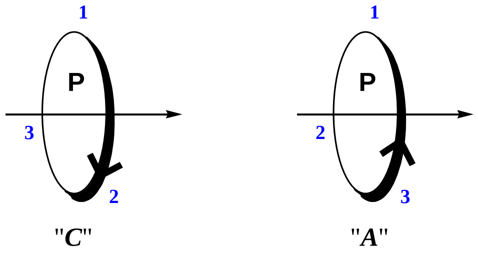

Figure S22. The *steering-wheel* system.

In the case of octahedrons (except those bearing several bis-chelate ligands for which the *Δ,Λ* is more appropriate), the oriented axis goes from the ligand with the highest priority (1) towards the *trans* ligand with the lowest possible priority. The ligands situated in the perpendicular plane are numbered according to the priority rules. The sense of rotation is then which goes from the ligand with the highest priority towards its immediate neighbor with the lowest priority.

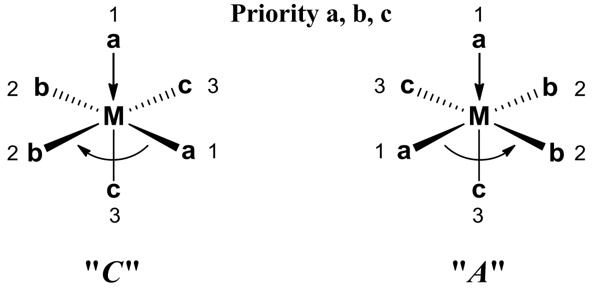

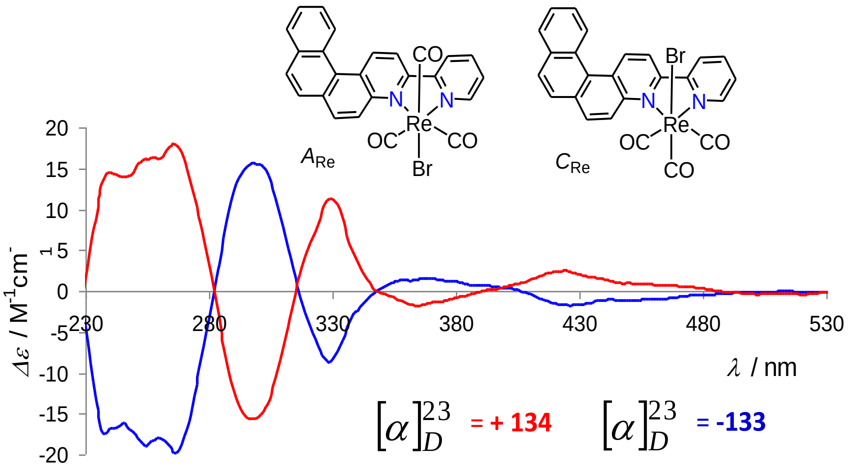

Figure S23. CD spectra of enantiopure complexes (**1a**)Re(CO)$_3$Br in CH$_2$Cl$_2$ (*C* 5. 10^{-5} M).

^{1} H NMR spectra

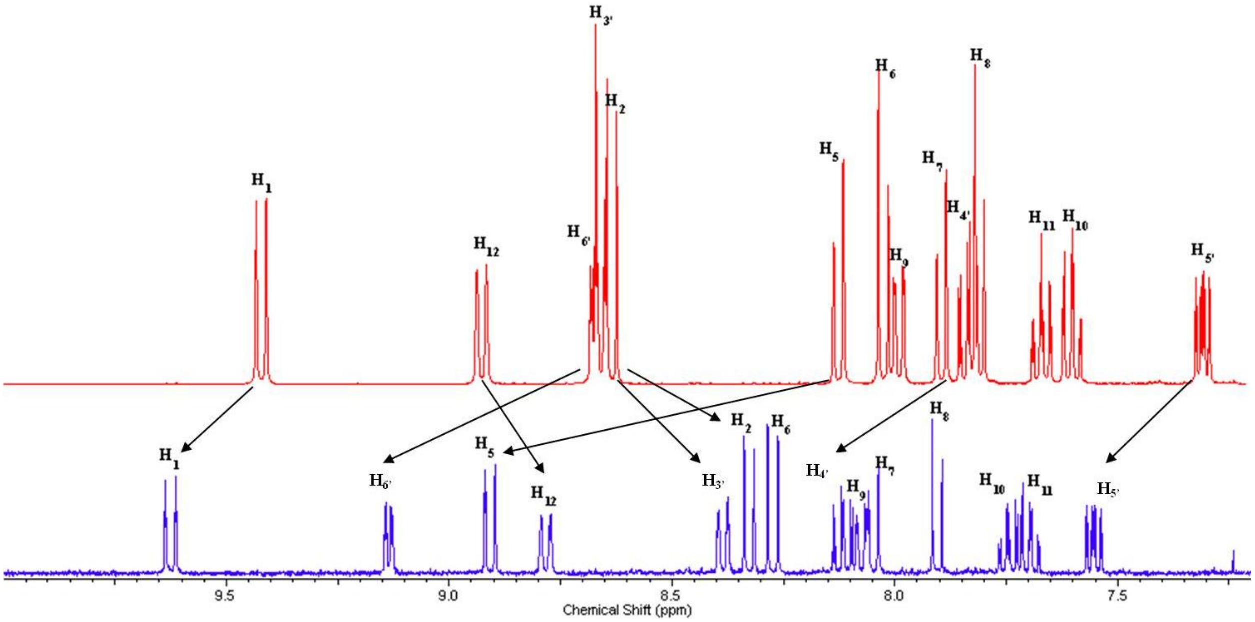

Figure S24. ^{1}H NMR spectra of ligand **1a** (red) and (**1a**)Re(CO)$_3$Cl (**2a**, blue) in CD_2Cl_2 (400 MHz)

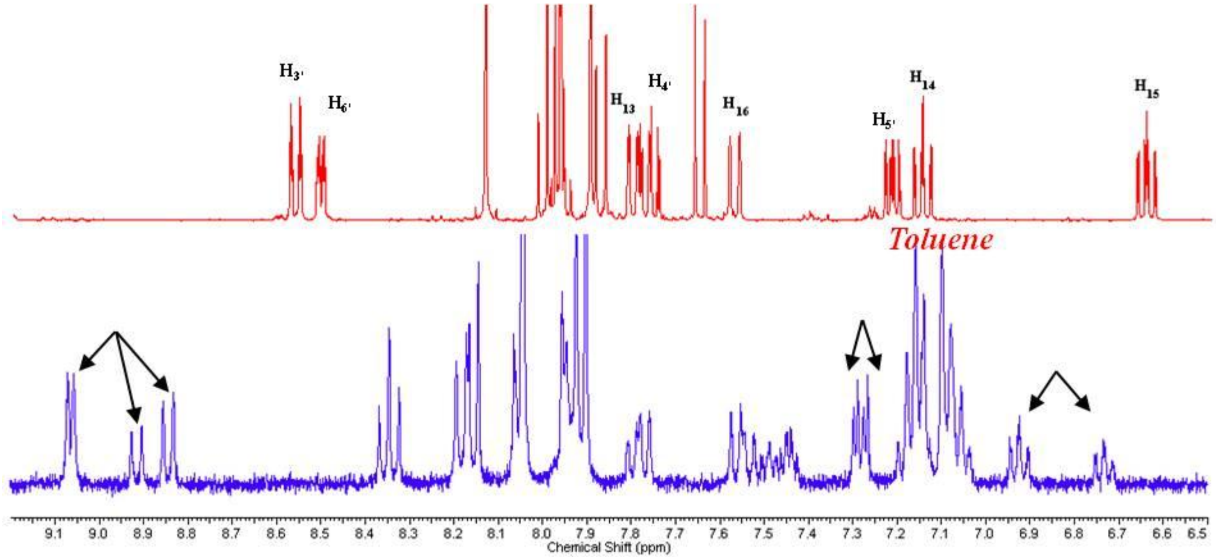

Figure S25. ^{1}H NMR spectra of H_6-bpy **1b** (red) and crude mixture of (**1b**)Re(CO)$_3$Cl (**2b^{1,2}**, blue) in CD_2Cl_2 (400 MHz)

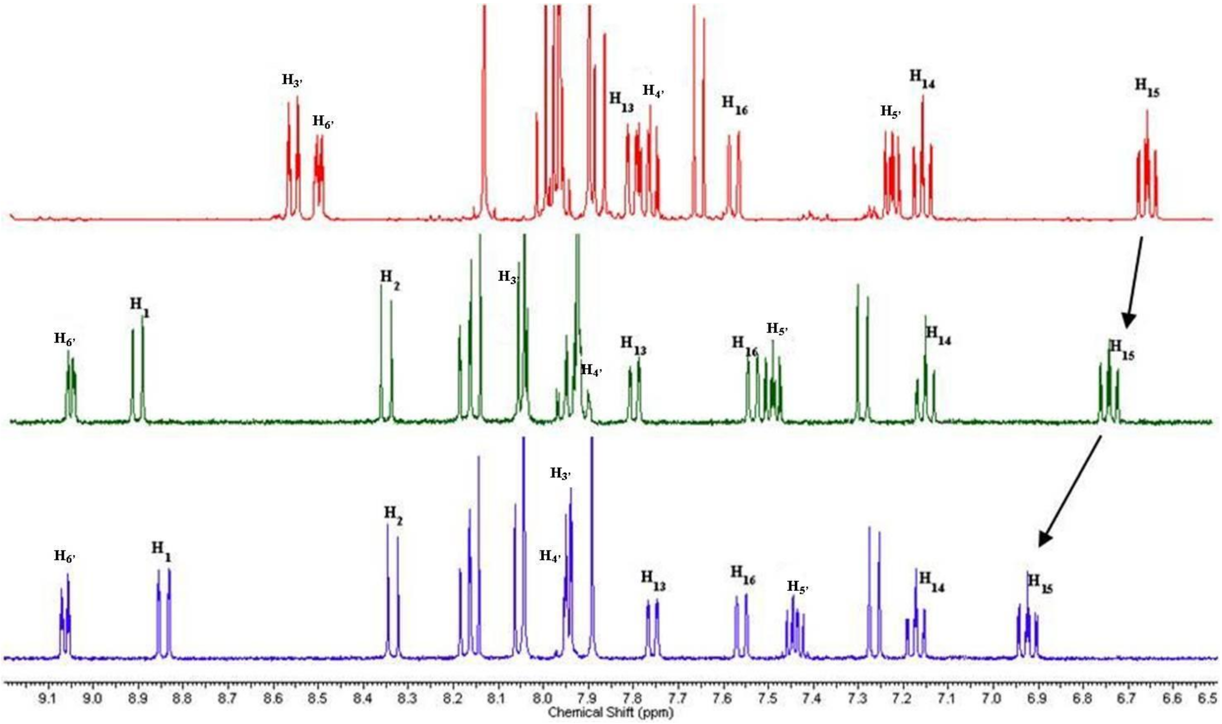

Figure S26. ^{1}H NMR spectra of H$_6$-bpy **1b** (red), **2b^1** (green) and **2b^2** (blue) in CD$_2$Cl$_2$ (400 MHz).

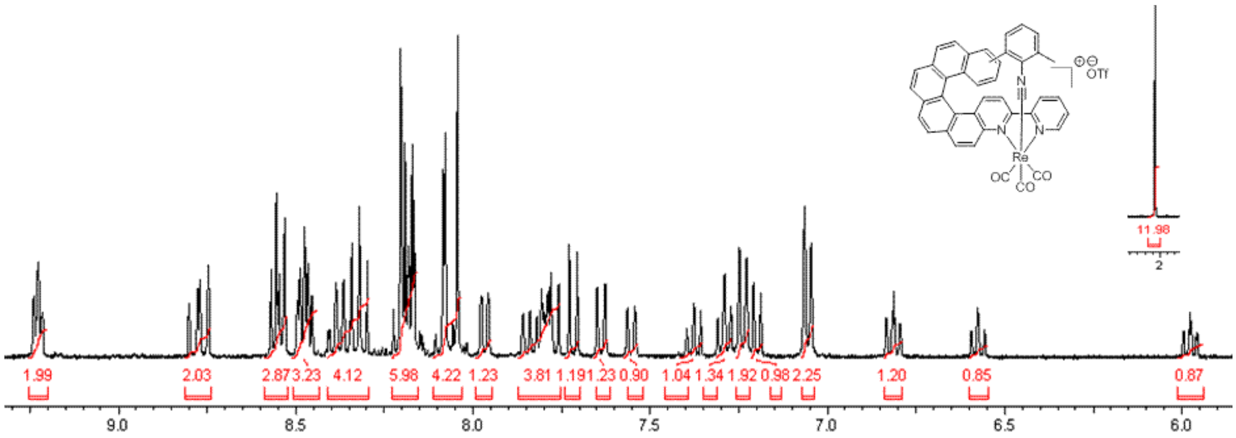

Figure S27. ^{1}H NMR spectra of **3b^{1,2}** in CD$_2$Cl$_2$ (400 MHz).

Non-polarised luminescence measurements

Instrumentation

Absorption spectra were measured on a Biotek Instruments XS spectrometer, using quartz cuvettes of 1 cm path length. Steady-state luminescence spectra were measured using a Jobin Yvon FluoroMax-2 spectrofluorimeter, fitted with a red-sensitive Hamamatsu R928 photomultiplier tube; the spectra shown are corrected for the wavelength dependence of the detector, and the quoted emission maxima refer to the values after correction. Samples for emission measurements were contained within quartz cuvettes of 1 cm path length modified with appropriate glassware to allow connection to a high-vacuum line. Degassing was achieved via a minimum of three freeze-pump-thaw cycles whilst connected to the vacuum manifold; final vapour pressure at 77 K was $< 5 \times 10^{-2}$mbar, as monitored using a Pirani gauge. Luminescence quantum yields were determined using $[Ru(bpy)_3]Cl_2$ in degassed aqueous solution as the standard ($\Phi_{lum} = 0.042$); estimated uncertainty in Φ_{lum} is ± 20% or better, except where indicated otherwise. Luminescence lifetimes < 10 μs were measured by time-correlated single-photon counting, following excitation at 374.0 nm with an EPL-375 pulsed-diode laser. The emitted light was detected at 90° using a Peltier-cooled R928 PMT after passage through a monochromator. Lifetimes > 10 μs were measured using the same detector in multichannel scaling mode following excitation with a microsecond pulsed xenon lamp. The estimated uncertainty in the quoted lifetimes is ± 10% or better.

Table S12. Emission maxima, quantum yields and lifetimes from degassed solution.

Compound	**Absorption** λ_{max} **/ nm (ε / M^{-1}cm^{-1})**	**Emission** λ_{max} **/ nm**	**Φ**	**τ / ns**$^{(b)}$	**Emission 77K**$^{(c)}$	
					λ_{max} **/ nm**	**τ / ns**
2a$^{(a)}$	243 (34500), 273 (30300), 318 (30300), 330 (43200), 398 (12700)	678	0.0011	25	550, 596, 644 sh	7900
3a$^{(a)}$	251 (54900), 273 (51900), 326sh (35900), 337 (46600), 403 (14600), 422 (15200)	585, 618	0.16	67000 [1200]	553, 600, 649	101000
4a$^{(a)}$	248 (35700), 280 (34200), 327sh (27300), 338 (37700), 408 (13500), 422 (13900)	595, 623	0.083	$11500^{)}$ [1200]	553, 599, 649	74000
2b$^{2(a)}$	237 (59800), 278 (65000), 305sh (36300), 344 (26300), 418 (11000), 445 (10200)	673	0.0016	33	554, 601, 654sh	43000
2b$^{1(a)}$	236 (45900), 277 (49900), 307 (28200), 339 (21300), 420 (7960), 444 (7300)	680	0.0013	27	560, 605, 654sh	46000
3b$^{1,2(a)}$	272 (48000), 339 (17600), 444 (5600)	598	0.06	79000 [1100]	560, 607, 660	210000

(a) In dichloromethane at 298 ± 3K, except where indicated otherwise. *(b)* In degassed solution. τ values in parentheses are those in air-equilibrated solution. (*c*) Data at 77 K recorded in diethyl ether / isopentane / ethanol (2:2:1 v/v).

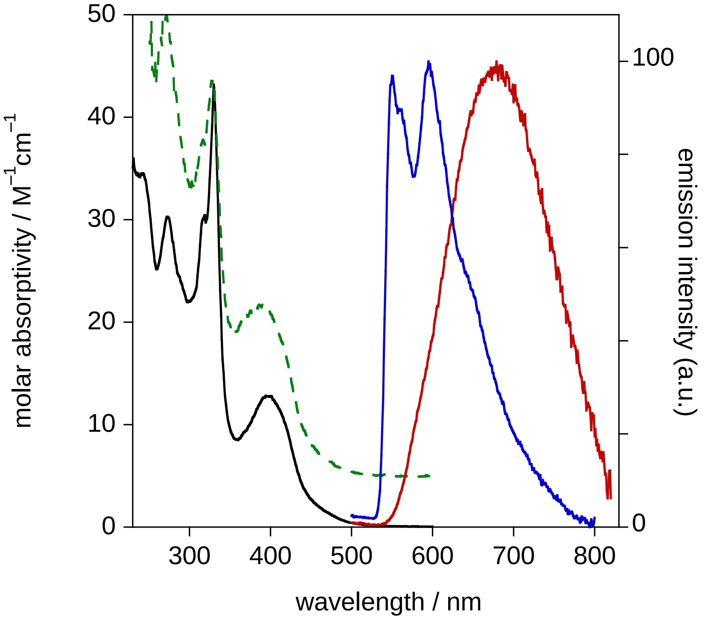

Figure S28. Spectra of **2a**: absorption (black line), emission (red line) and excitation (green dashed line) spectra at room temperature in CH_2Cl_2; emission spectrum in diethyl ether / isopentane / ethanol (2:2:1 v/v) at 77 K (blue line).

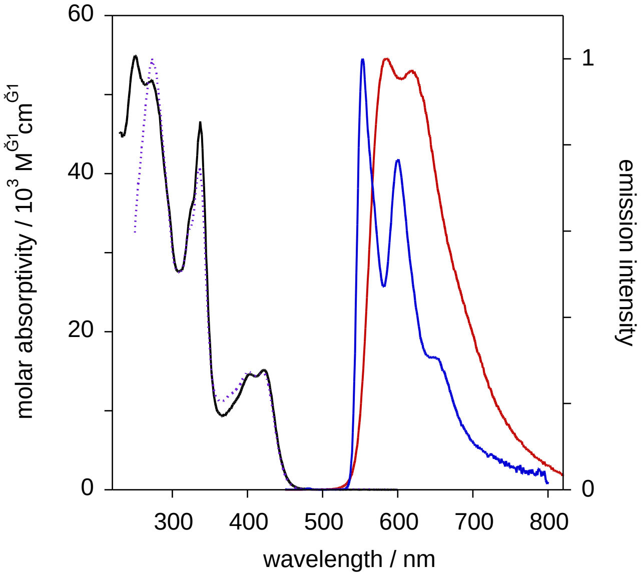

Figure S29. Spectra of **3a**: absorption (black line), emission (red line) and excitation (purple dashed line) spectra at room temperature in CH_2Cl_2; emission spectrum in diethyl ether / isopentane / ethanol (2:2:1 v/v) at 77 K (blue line).

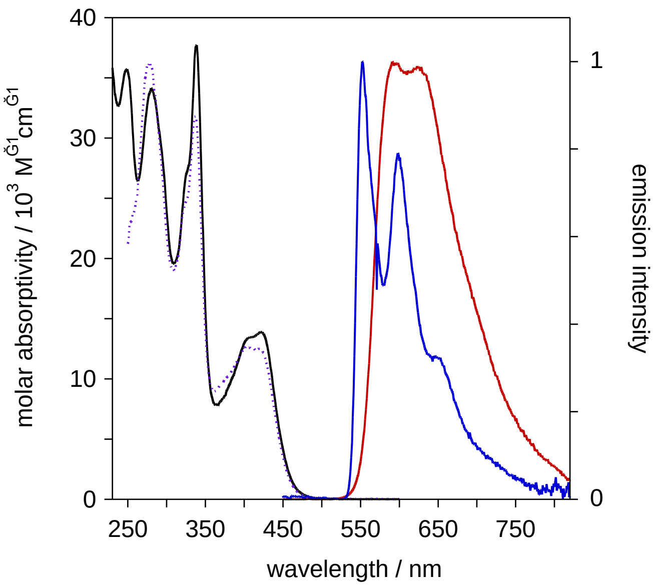

Figure S30. Spectra of **4a**: absorption (black line), emission (red line) and excitation (purple dashed line) spectra at room temperature in CH_2Cl_2; emission spectrum in diethyl ether / isopentane / ethanol (2:2:1 v/v) at 77 K (blue line).

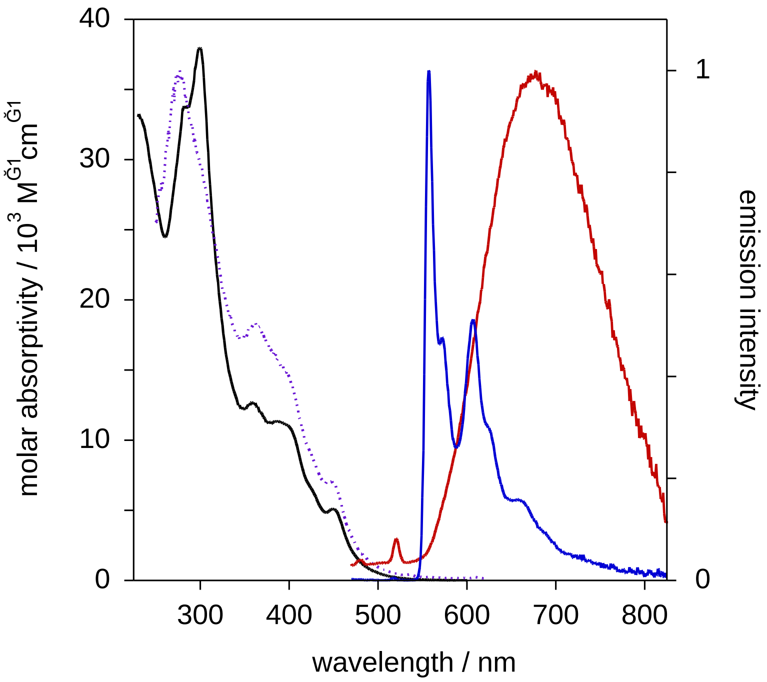

Figure S31. Spectra of **2b**[1]: absorption (black line), emission (red line) and excitation (purple dashed line) spectra at room temperature in CH_2Cl_2; emission spectrum in diethyl ether / isopentane / ethanol (2:2:1 v/v) at 77 K (blue line).

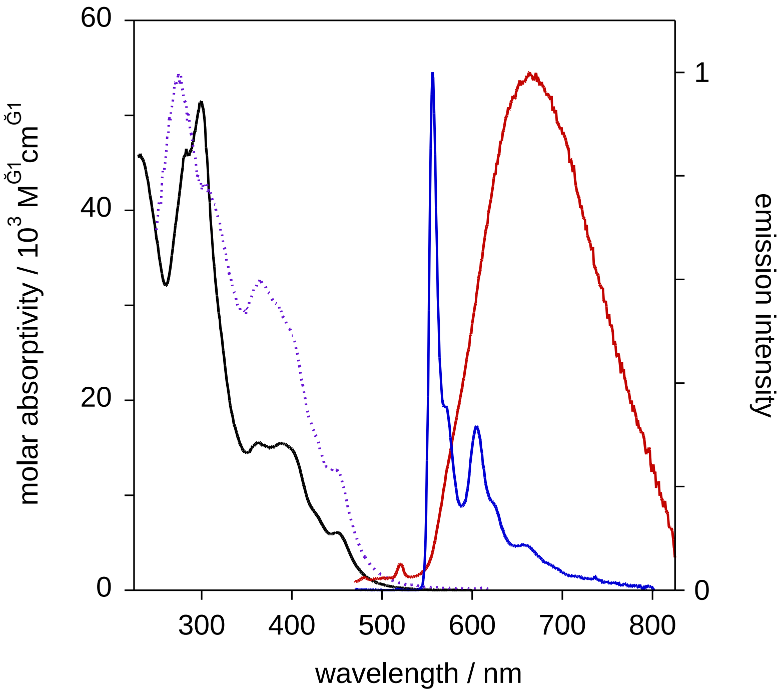

Figure S32. Spectra of **2b**^{2}: absorption (black line), emission (red line) and excitation (purple dashed line) spectra at room temperature in CH_2Cl_2; emission spectrum in diethyl ether / isopentane / ethanol (2:2:1 v/v) at 77 K (blue line).

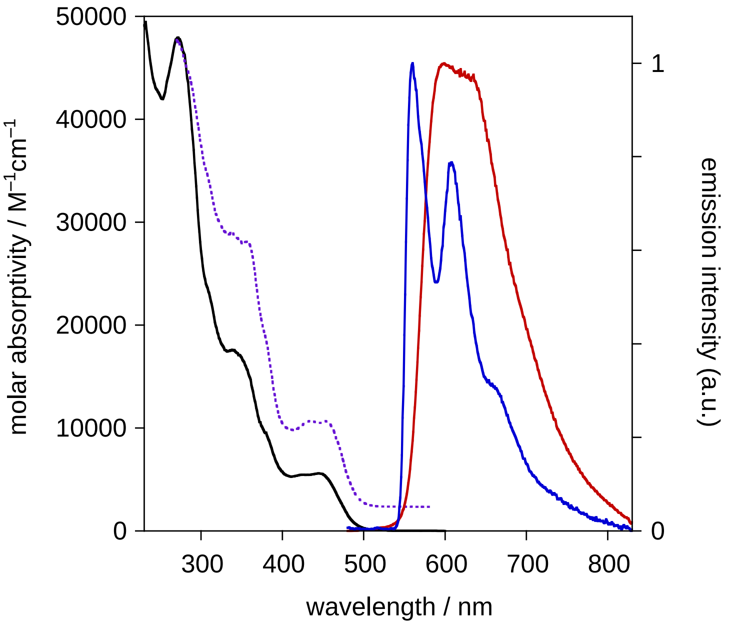

Figure S33. Spectra of **3b**^{1,2}: absorption (black line), emission (red line) and excitation (green dashed line) spectra at room temperature in CH_2Cl_2; emission spectrum in diethyl ether / isopentane / ethanol (2:2:1 v/v) at 77 K (blue line).

X-ray crystallographic data

ORTEP diagrams with ellipsoids at 50% probability of (±)-**3a**, (±)-**4a**, (±)-**2b^2**

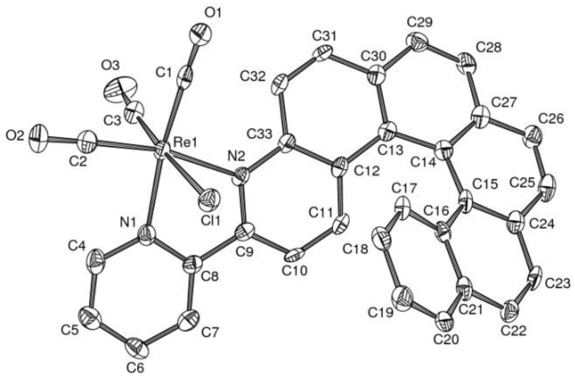

(±)-2b^2

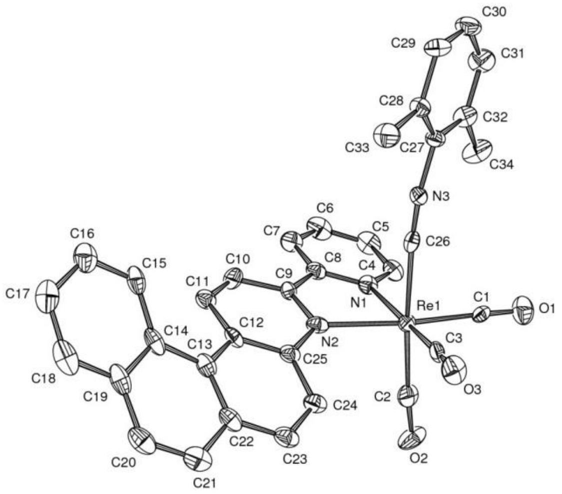

(±)-3a

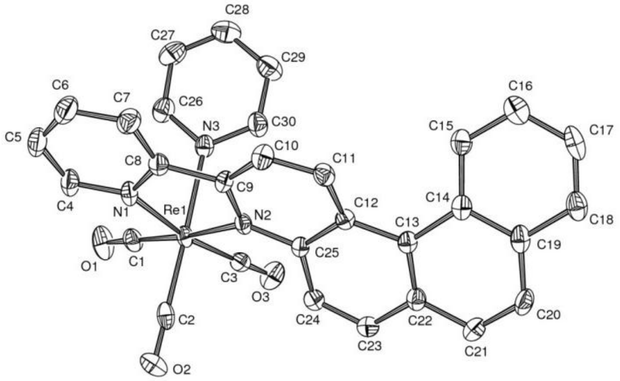

(±)-4a

Table S13. X-ray crystallographic data of complexes (±)-**2b**^{2}, (±)-**3a** and (±)-**4a**

	(±)-4a	**(±)-3a**	**(±)-2b^{2}**
Empirical Formula	$C_{32}H_{23}BCl_4F_4N_3O_3Re$	$C_{36.50}H_{25}Cl_3F_6N_3O_3PRe$	$C_{67}H_{40}Cl_2N_4O_7Re_2$
CCDC number	939180	942143	857156
Formula Weight	912.34	991.12	1456.33
Temperature (K)	140(2)	140(2)	140(2)
Wavelenght (Å)	0.71073	0.71073	0.71073
Crystal system	Monoclinic	Orthorhombic	Monoclinic
Space Group	$P2_1/n$	*F*dd2	$P2_1/c$
a (Å)	10.8540(2)	22.7551(3)	15.6700(2)
b (Å)	24.7778(3)	54.8820(10)	16.5072(3)
c (Å)	13.4316(2)	11.6412(2)	21.2401(4)
α (Å)	90	90.00	90
β (Å)	110.589(2)	90)	96.244(2)
γ (Å)	90	90.00	90
Volume (Å^{3})	3381.54(9)	14538.1(4)	5461.54(16)
Z	4	16	4
Color	yellow	yellow	yellow
$\rho_{\text{calculated}}$ (g.cm^{-3})	1.792	1.811	1.771
Absorption coefficient (mm^{-1})	3.970	3.681	4.589
F(000)	1776	7744	2840
Crystal size (mm)	0.323 * 0.216 * 0.149	0.191 * 0.169 * 0.067	0.203 * 0.143 * 0.059
θ range for data collection (º)	2.59 to 27.00	2.70 to 27.5	2.62 to 27.00
Tmin	0.35246	0.62986	0.505
Tmax	0.82193	0.81351	0.768
Limiting indices	$-11 \leq h \leq 13$ $-31 \leq k \leq 31$ $-17 \leq l \leq 11$	$-29 \leq h \leq 25$ $-70 \leq k \leq 69$ $-14 \leq l \leq 14$	$-19 \leq h \leq 20$ $-21 \leq k \leq 21$ $-27 \leq l \leq 27$
Data completeness	99.8% (θ = 27.00º)	99.9% (θ = 27.00º)	99.8% (θ = 27.00º)
Reflections collected	23796	28698	43976
Reflections unique	7355 [R(int) = 0.0351]	7488 [R(int) = 0.0335]	11893 [R(int) = 0.0734]
Data / restraints / parameters	7355 / 0 / 433	7488 / 1 / 469	11893 / 0 / 729
Goodness-of-fit on F^{2}	1.044	0.937	0.868
Final *R* indices [$I>2\sigma(I)$]	R1 = 0.0249, wR2 = 0.0616	R1 = 0.0320, wR2 = 0.0775	R1 = 0.0381, wR2 = 0.0697
R indices (all data)	R1 = 0.0386, wR2 = 0.0647	R1 = 0.0373, wR2 = 0.0790	R1 = 0.0803, wR2 = 0.0749
Largest diff peak and hole (e Å^{-3})	1.036 and -0.619	1.465 and -0.940	2.006 and -1.098

CPL measurements

The circularly polarized luminescence (CPL) and total luminescence spectra were recorded on an instrument described previously,[20] operating in a differential photon-counting mode. The light source for excitation was a continuous wave 1000 W xenon arc lamp from a Spex Fluorolog-2 spectrofluorimeter, equipped with excitation and emission monochromators with dispersion of 4 nm/mm (SPEX, 1681B). To prevent artifacts associated with the presence of linear polarization in the emission,[21] a high quality linear polarizer was placed in the sample compartment, and aligned so that the excitation beam was linearly polarized in the direction of emission detection (z-axis). The key feature of this geometry is that it ensures that the molecules that have been excited and that are subsequently emitting are isotropically distributed in the plane (x,y) perpendicular to the direction of emission detection. The optical system detection consisted of a focusing lens, long pass filter, and 0.22 m monochromator. The emitted light was detected by a cooled EMI-9558B photomultiplier tube operating in photo-counting mode. All measurements were performed with quartz cuvettes with a path length of 1.0 cm.

References

---

[1] *a*) S. Graule, M. Rudolph, N. Vanthuyne, J. Autschbach, C. Roussel, J. Crassous, R. Réau, *J. Am. Chem. Soc.* 2009, **131**, 3183; *b*) L. Norel, M. Rudolph, N. Vanthuyne, J. A. G. Williams, C. Lescop, C. Roussel, J. Autschbach, J. Crassous, R. Réau, *Angew. Chem. Int. Ed.* 2010, **49**, 99; *c*) E. Anger, M. Rudolph, C. Shen, N. Vanthuyne, L. Toupet, C. Roussel, J. Autschbach, J. Crassous, R. Réau, *J. Am. Chem. Soc.* 2011, **133**, 3800; *d*) E. Anger, M. Srebro, N. Vanthuyne, L. Toupet, S. Rigaut, C. Roussel, J. Autschbach, J. Crassous, R. Réau, *J. Am. Chem. Soc.* 2012, **134**, 15628; *e*) C. Shen, E. Anger, M. Srebro, N. Vanthuyne, L. Toupet, C. Roussel, J. Autschbach, R. Réau, J. Crassous, *Chem. Eur. J.* 2013, **19**, 16722.

[2] *a*) TURBOMOLE V5.7.1 2005 and V6.5 2013, a development of University of Karlsruhe and Forschungszentrum Karlsruhe GmbH, 1989-2007, TURBOMOLE GmbH, since 2007; available from http://www.turbomole.com; *b*) R. Ahlrichs, M. Bär, M. Häser, H. Horn, C. Kölmel, *Chem. Phys. Lett.* 1989, **162**, 165; *c*) F. Furche, R. Ahlrichs, C. Hättig, W. Klopper, M. Sierka, F. Weigend, *WIREs Comput. Mol. Sci.* 2014, **4**, 91.

[3] *a*) A. D. Becke, *Phys. Rev. A* 1988, **38**, 3098; *b*) J. P. Perdew, *Phys. Rev. B* 1986, **33**, 8822–8824; *c*) J. P. Perdew, *Phys. Rev. B* 1986, **34**, 7406.

[4] *a*) C. Lee, W. Yang, R. G. Parr, *Phys. Rev. B* 1988, **37**, 785; *b*) A. D. Becke, *J. Chem. Phys.* 1993, **98**, 1372.

[5] *a*) A. Schäfer, H. Horn, R. Ahlrichs, *J. Chem. Phys.* 1992, **97**, 2571; *b*) K. Eichkorn, F. Weigend, O. Treutler, R. Ahlrichs, *Theor. Chem. Acc.* 1997, **97**, 119.

[6] D. Andrae, U. Häußermann, M. Dolg, H. Stoll, H. Preuß, *Theoret. Chim. Acta* 1990, **77**, 123.

[7] *a*) A. Klamt, G. J. Schüürmann, *J. Chem. Soc., Perkin Trans. 2* 1993, 799; *b*) A. Klamt, *J. Phys. Chem.* 1996, **100**, 3349; *c*) G. Scalmani, M. J. Frisch, B. Mennucci, J. Tomasi, R. Cammi, V. Barone, *J. Chem. Phys.* 2006, **124**, 094107.

[8] J. Autschbach, T. Ziegler, S. J. A. van Gisbergen, E. J. Baerends, *J. Chem. Phys.* 2002, **116**, 6930.

[9] Gaussian 09, Revision D.01, M. J. Frisch, G. W. Trucks, H. B. Schlegel, G. E. Scuseria, M. A. Robb, J. R. Cheeseman, G. Scalmani, V. Barone, B. Mennucci, G. A. Petersson, H. Nakatsuji, M. Caricato, X. Li, H. P. Hratchian, A. F. Izmaylov, J. Bloino, G. Zheng, J. L. Sonnenberg, M. Hada, M. Ehara, K. Toyota, R. Fukuda, J. Hasegawa, M. Ishida, T. Nakajima, Y. Honda, O. Kitao, H. Nakai, T. Vreven, J. A. Montgomery, Jr., J. E. Peralta, F. Ogliaro, M. Bearpark, J. J. Heyd, E. Brothers, K. N. Kudin, V. N. Staroverov, R. Kobayashi, J. Normand, K. Raghavachari, A. Rendell, J. C. Burant, S. S. Iyengar, J. Tomasi, M. Cossi, N. Rega, J. M. Millam, M. Klene, J. E. Knox, J. B. Cross, V. Bakken, C. Adamo, J. Jaramillo, R. Gomperts, R. E. Stratmann, O. Yazyev, A. J. Austin, R. Cammi, C. Pomelli, J. W. Ochterski, R. L. Martin, K. Morokuma, V. G. Zakrzewski, G. A. Voth, P. Salvador, J. J. Dannenberg, S. Dapprich, A. D. Daniels, Ö. Farkas, J. B. Foresman, J. V. Ortiz, J. Cioslowski, and D. J. Fox, Gaussian, Inc., Wallingford CT, 2009.

[10] *a*) J. Tomasi, B. Mennucci, R. Cammi, *Chem. Rev.* 2005, **105**, 2999; *b*) R. Cammi, B. Mennucci, J. Tomasi, *J. Phys. Chem. A* 2000, **104**, 5631; *c*) M. Cossi, V. Barone, *J. Chem. Phys.* 2001, **115**, 4708.

---

[11] *a*) I. Tamm, *J. Phys. USSR* 1945, **9**, 449; *b*) S. M. Dancoff, *Phys. Rev.* 1950, **78**, 382; *c*) S. Hirata, M. Head-Gordon, *Chem. Phys. Lett.* 1999, **314**, 291; *d*) M. J. G. Peach, M. J. Williamson, D. J. Tozer, *J. Chem. Theory Comput.* 2011, **7**, 3578; *e*) M. J. G. Peach, D. J. Tozer, *J. Phys. Chem. A* 2012, **116**, 9783; *f*) M. J. G. Peach, N. Warner, D. J. Tozer, *Mol. Phys.* 2013, **111**, 1271.

[12] F. Wang, T. Ziegler, *J. Chem. Phys.* 2005, **123**, 154192.

[13] F. Wang, T. Ziegler, E. van Lenthe, S. J. A. van Gisbergen, E. J. Baerends, *J. Chem. Phys.* 2005, **122**, 204103.

[14] *a*) ADF2013, SCM, Theoretical Chemistry, Vrije Universiteit, Amsterdam, The Netherlands, http://www.scm.com; *b*) C. F. Guerra, J. G. Snijders, G. te Velde, E. J. Baerends, *Theor. Chem. Acc.* 1998, **99**, 391; *c*) G. te Velde, F. M. Bickelhaupt, E. J. Baerends, C. F. Guerra, S. J. A. van Gisbergen, J. G. Snijders, T. Ziegler, *J. Comput. Chem.* 2001, **22**, 931.

[15] *a*) P. J. Stephens, F. J. Devlin, C. F. Chabalowski, M. J. Frisch, *J. Phys. Chem.* 1994, **98**, 11623; *b*) A. D. Becke, *J. Chem. Phys.* 1993, **98**, 5648.

[16] C. C. Pye, T. Ziegler, *Theor. Chem. Acc.* **1999**, *101*, 396–408.

[17] K. Mori, T. P. M. Goumans, E. van Lenthe, F. Wang, *Phys. Chem. Chem. Phys.* 2014, **16**, 14523.

[18] N. Saleh, B. Moore, II, M. Srebro, N. Vanthuyne, L. Toupet, J. A. G. Williams, C. Roussel, K. K. Deol, G. Muller, J. Autschbach, J. Crassous , *Chem. Eur. J.*, 2015, **21**, 1673.

[19] *a)* R. S. Cahn, C. K. Ingold, V. Prelog, *Experientia*, 1956, **12**, 81; *b)* R. S. Cahn, C. K. Ingold, V. Prelog, *Angew. Chem. Int. Ed.* 1966, **5**, 385; *c)* V. Prelog, G. Helmchen, *Angew. Chem. Int. Ed.*, 1982, **94**, 614; *d)* T. Damhus, C. E. Schäffer, *Inorg. Chem.* 1983, **22**, 2406.

[20] E. Brunet, L. Jiménez, M. de Victoria-Rodriguez, V. Luu, G. Muller, O. Juanes, J. C. Rodríguez-Ubis, *Microporous and Mesoporous Mater.* 2013, **169**, 222, and references therein.

[21] H. P. J. M. Dekkers, P. F. Moraal, J. M. Timper, J. P. Riehl, *Appl. Spectrosc.* 1985, **39**, 818.